Aus dem Institut für Medizinische Immunologie
der Medizinischen Fakultät Charité – Universitätsmedizin Berlin

DISSERTATION

Novel MR Tools Highlight Brain Barrier Alterations in a Mouse Model of Multiple Sclerosis

zur Erlangung des akademischen Grades
Doctor medicinae (Dr. med.)

vorgelegt der Medizinischen Fakultät
Charité – Universitätsmedizin Berlin

von

Laura Hanke Vela

aus Bonn

Datum der Promotion: 21. Juni 2020

PREFACE

Results in this dissertation have partly been published in the paper:

Application of Europium-Doped Very Small Iron Oxide Nanoparticles to Visualize Neuroinflammation with MRI and Fluorescence Microscopy. Millward, J.M., A. Ariza de Schellenberger, D. Berndt, L. Hanke-Vela, E. Schellenberger, S. Waiczies, M. Taupitz, Y. Kobayashi, S. Wagner, and C. Infante-Duarte, *Neuroscience,* 2017.

Furthermore, a second portion of the results presented in this work is currently in revision process with a paper in collaboration with S. Wang, J.M. Millward et al.

TABLE OF CONTENTS

LIST OF TABLES

LIST OF FIGURES

INDEX OF ABBREVIATIONS

N

O

P

R

S

T

U

V

Z

ABSTRACT (DEUTSCH)

Aktuelle Forschungsergebnisse zur Multiplen Sklerose (MS) und dem dazugehörigen Tiermodell, Experimentelle autoimmune Enzephalomyelitis (EAE), unterstreichen die Rolle von Hirnschranken für den Beginn und die Aufrechterhaltung der Neuroinflammation. In den letzten Jahren rückte die Suche nach Visualisierungsmethoden beeinträchtigter Schranken als Methode zur frühen Diagnostik und zum Verständnis grundlegender pathophysiologischer Prozesse der Neuroinflammation in den Fokus. Gängige Bildgebungsmethoden, die Gadolinium-basierte Kontrastmittel benutzen, haben verschiedene Nachteile, da sie weder alle Aspekte dysfunktionaler Blut-Hirn-Schranken zeigen, noch eindeutige Klarheit über potentielle toxische Effekte wiederholter Kontrastmittelgaben besteht. Unsere Arbeitsgruppe hat sich in den letzten Jahren der Erforschung neuartiger Magnetresonanz (MR) - Bildgebungsmethoden gewidmet, die es erlauben, in vivo Untersuchungen mit histopathologischen und molekularbiologischen Einsichten zu vereinen. In der vorliegenden Arbeit nutzten wir eine neue Art von elektromagnetischen Nanopartikeln, die Europium-dotierten sehr kleinen Eisenoxid Partikel (engl. *Europium-doped very small iron oxide particles* = Eu-VSOP), um Störungen der Blut-Liquor-Schranke am Plexus choroideus (CP) zu visualisieren. Dafür führten wir, nach intravenöser Gabe von Eu-VSOP, zu verschiedenen Zeitpunkten der EAE MR-Aufnahmen durch und analysierten fluoreszenzmikroskopisch die dazugehörigen histopathologischen Schnitte. Unsere Ergebnisse zeigen, dass Eu-VSOP die in vivo Visualisierung von Hirnschrankenstörungen und neuroinflammatorischen Prozessen ermöglichen und erlauben, diese post mortem mit Veränderungen des CP zu verknüpfen.

Unsere Forschungsgruppe hat in vorhergehenden Studien mit MR-Elastographie (MRE) in MS und EAE gezeigt, dass chronisch-entzündliche Erkrankungen des zentralen Nervensystems (ZNS) mit einem Verlust der Steifheit des Hirngewebes einhergehen. Im zweiten Teil der vorliegenden Studie führten wir nun MRE-Messungen in EAE-Mäusen durch, um mittels Veränderungen mechanischer Eigenschaften des Hirngewebes Störungen der Blut-Hirn-Schranke (BHS) zu demaskieren. Wir konnten zeigen, dass jene Hirnregionen, die stärker von der Neuroinflammation betroffen sind, besonders starke Verluste der Steifigkeit präsentieren und dass diese Veränderungen, anders als bei Verwendung gadoliniumhaltiger Kontrastmittel, mit dem klinischen Verlauf korrelieren. Weiterhin konnten wir beweisen, dass perivaskuläre Läsionen, in denen die BHS gestört ist, ein Remodeling mit Aggregaten des Extrazellulärmatrix-Proteins Fibronektin (Fn) durchlaufen, und dass die Genexpression dieses

Proteoglykans mit MRE-Veränderungen korreliert. Damit stellt diese Studie eine Grundlage zur Visualisierung von Hirnschrankenstörungen als zentraler pathophysiologischer Prozess zur Entstehung neuroinflammatorischer Läsionen sowie zur Implementierung neuer MR-basierter Bildgebungsmethoden als Diagnosemittel der MS dar.

ABSTRACT (ENGLISH)

Previous studies on multiple sclerosis (MS) and its animal model experimental autoimmune encephalomyelitis (EAE) have highlighted the role of brain-barrier breakdown for the initiation and maintenance of neuroinflammation. Prior research generally confirms that visualization of barrier-disruption is of major interest for an early diagnostic of neuroinflammatory diseases. However, common contrast-agents like gadolinium-based contrast agents (GBCA) have important limitations as they don't accurately show all aspects of brain-barrier breakdown and recent reports point towards potential side effects of repeated gadolinium applications. In the last years, our group has applied novel magnetic resonance imaging (MRI) techniques to visualize more accurately neuroinflammation in vivo and to elucidate pathological pathways involved in disease development. In this study, we first used Europium-doped very small iron oxide particles (Eu-VSOP), a new kind of magnetic nanoparticles, to visualize alterations of the blood-cerebrospinal-fluid-barrier (BCSFB) at the site of the Choroid Plexus (CP) in a mouse model of MS. We performed MRI measurements in EAE mice at different phases of disease after injection of Eu-VSOP and analyzed histopathological correlates using fluorescent microscopy. Our results show the ability of Eu-VSOP to visualize BCSFB alterations and neuroinflammatory processes in vivo and to connect them to histopathological findings of a compromised barrier at the level of the CP.

In the second part of the study, we performed MRE measurements in EAE mice to assess alterations of brain mechanical properties associated to blood-brain-barrier (BBB) breakdown. We previously demonstrated using MR-elastography (MRE) in both MS and EAE that inflammation led to a reduction of brain stiffness. Here, we demonstrated that highly active inflammatory areas are especially prone to softening, and that, in contrast to GBCA, MRE alterations correlate with clinical disability. We further demonstrate that perivascular areas, where BBB is disrupted, undergo a process of tissue remodeling, characterized by the presence of aggregates of the extracellular matrix protein fibronectin (Fn). Interestingly, Fn expression correlates with MRE changes. Therefore, this study contributes to better understanding the pathophysiological processes around brain barrier breakdown as a central step in the dynamic of lesion formation and to the development of novel MRI techniques as a diagnostic tool for MS.

DISSERTATION

Introduction

Multiple Sclerosis (MS) is a chronic inflammatory and demyelinating disease of the central nervous system (CNS). Approximately 2.5 million people worldwide and 122.000 in Germany are affected by this autoimmune disease that represents the most common non-traumatic cause of disability in young adults. The average onset age is between 20 and 40 years and 50% of patients require the permanent use of a wheelchair by 25 years of disease history, often leading to early retirement and comorbidity. Thus, MS poses a major personal and socioeconomic burden [1].

MS prevalence shows a north-south gradient, being more common in countries far from the equator, with small exceptions, for example in certain ethnic groups. Women are affected 2-3 times as often as men. During the last decades, MS incidence is increasing in high prevalence regions like northern Europe and North America, but also in regions traditionally less affected like Japan [2].

Prior research has thoroughly investigated the etiology of the disease, but the exact cause remains unclear. A multifactorial genesis is generally assumed, in which environmental factors influence the disease's outbreak in genetically susceptible individuals. The probability of suffering of the condition is higher in relatives of an affected person, and the risk increases among those more closely related. For identical twins, this risk reaches up to 30-50%. The strongest genetic risk factors seem to be genes coding for certain MHC-molecules, especially HLA-DRB1[3]. Although non-genetic factors are thought to have a comparably higher impact on the disease's development, it has been more difficult to enlighten them. Amidst environmental determinants associated to the disease, Epstein-Barr Virus infection, low levels of Vitamin D and cigarette smoking have been shown to play a role in the outbreak and, partly, also in the course of MS [4].

MS presents with a variety of clinical symptoms depending on the region of the CNS affected. Whereas first symptoms observed may be sensory or visual impairments, severe motoric dysfunctions and neurocognitive deficits often accumulate when MS progresses, accompanied by chronic fatigue and pain [5]. A first manifestation of neuroinflammation may be the clinical isolated syndrome (CIS), showing typical dysfunctions associated to demyelinating diseases but not yet fulfilling the McDonald criteria for spatiotemporal dissemination. Clinical findings as well as the course of disease are highly variant from patient to patient, but two major forms of MS can be observed: 85-90% of patients are affected by relapsing-remitting-MS (RR-MS) forms, where inflammatory exacerbations are followed by

periods of complete or partial recovery. Untreated, RR-MS commonly transitions into secondary-progressive-MS (SP-MS) by 10-20 years after diagnosis, from which on the disease progresses without clear episodes. About 10-15% of all patients present a primary-progressive-MS (PP-MS) from the beginning, with a steady increase of disability over time and an overall worse prognosis. However, due to the observation that classical categorization of MS clinical course does not sufficiently capture the phenotypical range of disease, recent propositions aim to subclassify types by disease activity and progression on serial imaging or other objective measurements to monitor inflammatory lesions [6] .

Multiple sclerosis is considered a CNS-specific immune-mediated disease in which self-reactive cells and antibodies lead to a destruction of myelin sheaths. Lesions, a hallmark of MS, are caused by infiltrating immune cells when blood-brain-barrier (BBB) disruption occurs, and are characterized by inflammation, demyelination, gliosis and neuroaxonal degeneration [7]. Several models have been implemented to understand this complex condition, but it is difficult to say how exactly the two main immunopathogenic models discussed until now contribute to shape the development of the disease [8].

In the peripheral model, autoreactive $CD4^+$ T Cells, activated through molecular mimicry or bystander activation in the periphery against myelin components, seem to infiltrate the CNS alongside with B cells and monocytes. This model is supported by genome-wide association studies in which immunological relevant genes were identified, indicating the implication of T-helper-cell differentiation in the pathogenesis of multiple sclerosis [9]. It is also consistent with the histology of MS lesions and cerebrospinal fluid (CSF) cytology in humans as well as with the model used to induce an MS-like disease in animal experiments, the experimental autoimmune encephalomyelitis (EAE). Autoreactive $CD4^+$ T helper (Th) 1 and Th17 cells from draining lymph nodes enter the blood circulation and transit to the CNS, where they cross the BBB or the blood-CSF-barrier (BCSFB) at the choroid plexus and eventually find their targets. But additional to infiltration of the CNS by activated autoreactive T cells, there seems to be a CNS-intrinsic process triggering disease development, less identified but likely to involve innate immunity, with infiltration of peripheral immune cells as a secondary step. In this second model, it is not yet clear what events could lead to the immune-activation in the CNS, although some hypothesis suggest neuroinflammation secondary to a still unknown CNS virus infection or as a reaction to processes linked to primary neurodegeneration, similar to the ones in neurodegenerative diseases as Alzheimers disease or Parkinsons [10].

After disruption of BBB and infiltration of the CNS, $CD4^+$ T cells are likely to drive the inflammatory process by activating resident cells, such as microglia and astrocytes and recruiting other immune cells, including CD8+ T cells, B cells, monocytes and mast cells from the peripheral blood. Inflammatory lesions are characterized by a disruption of BBB with tissue edema after release of proinflammatory molecules and proteases by T cells and cells of the innate immune system. T cells are largely seen in the perivascular space, especially in active disease, but they also infiltrate the CNS parenchyma in considerable amounts. However, damage of the target tissue, i.e. myelin sheaths, oligodendrocytes and axons, is most likely mediated by other immunological components, such as innate immune cells, complements and antibodies. These cells seem to play a role not only in visible lesions, but also in normal-appearing white matter (NAWM) lesions. Several studies have shown that at least in some regions, clear alterations of NAWM can be seen days to weeks before the formation of contrast-agent-enhancing lesions [11].

The post-inflammatory process is characterized by activation and beginning proliferation of astrocytes as well as activation of oligodendrocyte precursor cells (OPC), contributing to remyelination, which will however not generate the original thickness of the compact myelin. The proliferation and activation of glial cells (microglia, oligodendrocytes and astrocytes) causes repeated scarring, gliosis and sclerosis of lesions at multiple sites and timepoints, a process that has been name-giving for the condition [12].

To study MS pathogenesis, and especially neuroinflammation, the common animal model used is the EAE. In this model, animals (most often mice) injected with a myelin component (acting as an antigen) together with immune stimulants (adjuvants) develop a $CD4^+$ mediated autoimmune disease, sharing clinical and immunological similarities with MS. The disease developed differs depending on the immunization method and animal strain used. The acute mouse model of EAE is induced in susceptible animal strains by active immunization with myelin-related antigens such as myelin basic protein (MBP), myelin oligodendrocyte glycoprotein (MOG) or myelin proteolipid protein (PLP) emulsified in adjuvant[13]. SJL mice immunized with a PLP antigen develop a condition similar to RR-MS, with remission and relapses and consequent progressive limb paralysis. In this model, inflammation is primarily mediated by autoreactive T cells [14]. EAE in SJL mice is known to mostly affect cerebellum and to cause a diffuse inflammation, whereas animals of the C57/BL6 strain immunized with a MOG-peptide suffer a more pronounced spinal cord pathology (figure 1).

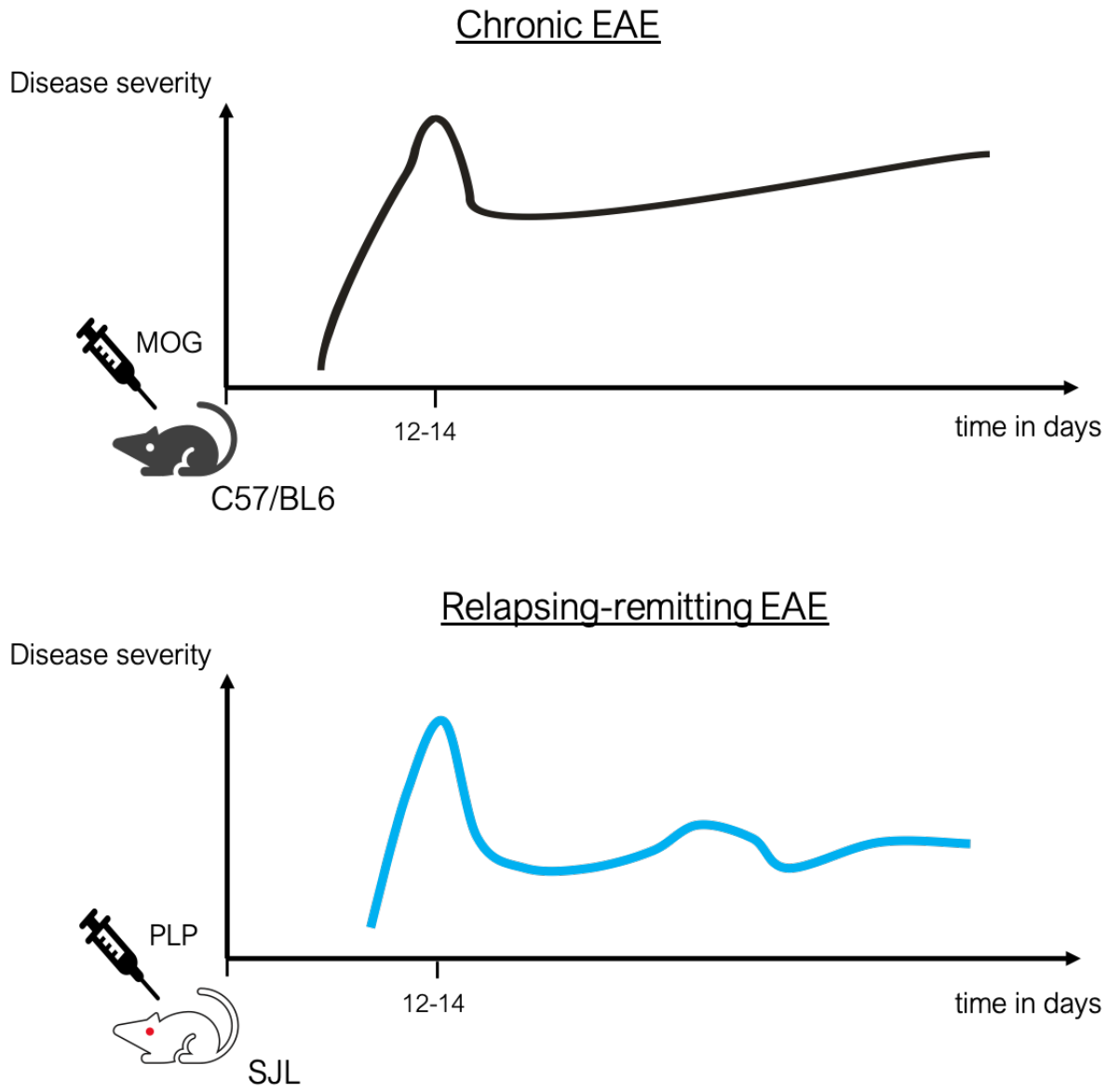

Figure 1. Variable disease progression in different EAE models. 57/BL6 mice develop a chronic-progressive EAE with peak around 13 days after immunization and focus on spinal cord after immunization with MOG. SJL animals are immunized with PLP in order to cause a relapsing-remitting EAE course affecting primarily the cerebellum. Adapted after Carmen Infante-Duarte.

It is widely accepted that disruption of the brain barriers is a crucial point in the pathogenesis of MS. In healthy individuals, the BBB helps maintaining the CNS tissue homeostasis by performing controlled metabolic exchanges through a tightly regulated cellular barrier, while impeding neurotoxic agents, potential pathogens and peripheral immune cells of infiltrating the CNS. Numerous cells are implicated in this complex phenomenon, amongst which endothelial cells, pericytes, astrocytes and the basement membrane form the neurovascular unit (NVU). The NVU represents all the components, cellular and molecular, that interact at the critical interface between the blood and the CNS and hence form a central element in inducing and

regulating the BBB [15]. In the initiation of neuroinflammation, disruption of BBB is partly provoked by Th1 and Th17 cells from the luminal side that produce proinflammatory cytokines and matrix metalloproteinases (MMPs), which open adherence and tight junctions and enable leukocyte diapedesis (fig. 2 A). The breakdown of the BBB with following infiltration of immune cells is tried to be assessed in MS therapies, such IFN-β blocking MMP-production or Natalizumab, a humanized antibody against VLA-4, which blocks the leukocyte migration through the BBB and reduces brain inflammation [16].

T cells can also access the CNS by crossing the BCSFB via the choroid plexus (CP), binding to CP endothelial cells [17]. To fully understand how these mechanisms are mediated by the CP, it is important to understand its function, structure and location. The CP is a villous structure floating inside the ventricles of the brain, whose main function is the production of CSF, although it also seems so be an interface between the CNS and the peripheral immune system. It consists of small vessels surrounded by epithelial cells, who are largely responsible for establishing the BCSFB. In contrast to the BBB, the BCSFB is formed by a leakier, fenestrated endothelium with apical tight junctions between the epithelial cells, filtrating the CSF out of the blood into the ventricles (fig. 2 B). Recent studies have shown that T cells use the CP to enter the CSF and disseminate into the meninges and perivascular spaces [18].

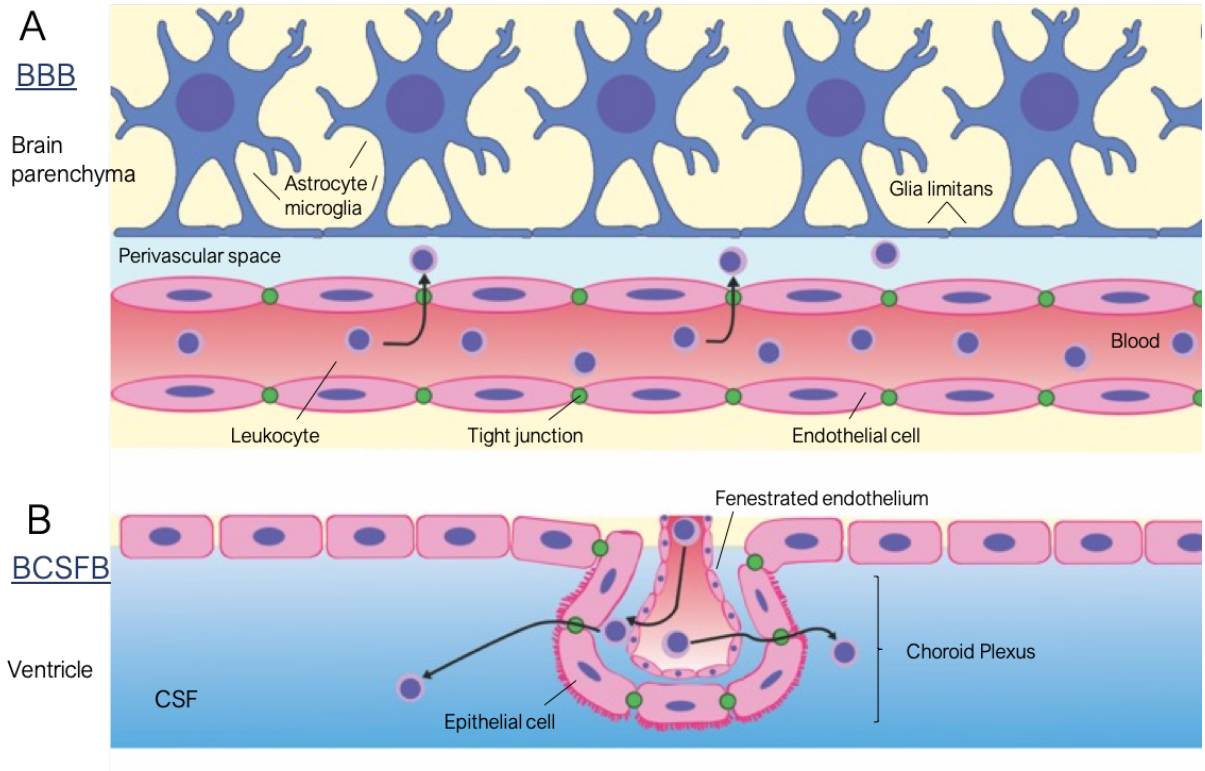

Figure 2. Migration of immune cells through brain barriers. Brain barriers are made of the endothelial BBB and the epithelial BCSFB. The BBB consists in a double protective layer: the endothelium with tight junctions and the glia limitans, made up of

the parenchymal basement membrane and the glia limitans, foot processes that are to 2/3 from astrocytes, 1/3 from microglia. In contrast to the CNS parenchyma, microvessels in the CP are fenestrated, allowing free diffusion and filtration of liquid between the blood and the CSF. The BCSFB is build of the CP epithelial cells with their unique tight junctions. In neuroinflammation, Th1 and Th17 cells invade the CNS parenchyma, the meninges and the CSF. For this purpose, they produce cytokines and MMPs in proximity of endothelial cells of microvessels to open tight junctions at both barriers and enable leukocyte diapedesis. Figure modified from [19]

Thus, if brain barriers and the CP are involved in the initiation of neuroinflammation, imaging of barrier breakdown and plexuses could help to better diagnose and understand the mechanisms happening during early disease stages. In fact, one typical localization of MS lesions is periventricular, indicating that the liquid filled cisterns are a gate by which immune cells reach the CNS. For now, the CP has been shown to be involved in early stages of disease, but it is unclear which role it plays during remission and relapse.

MS diagnostics have undergone considerable changes in criteria in the last two decades. Clinical impairment is widely measured with the extended disability status scale (EDSS), a score based on symptoms in eight functional systems, walking ability and activities of daily living. Today, it represents the most important measurement instrument to assess clinical disease progression in MS [5]. However, because tools as the EDSS have well known limitations, one of which is the small sensitivity in relatively low scores, additional methods of monitoring inflammation are used [20]. In MS patients clinical relapses correspond to the formation of active inflammatory lesions, usually forming around blood vessels or the ventricles, which can be visualized with contrast-enhanced magnetic resonance imaging (MRI). Although there is no single diagnostic test to recognize the condition, the McDonald criteria for MS, updated several times in recent years, reflect the diagnostic breakthrough of this imaging method. Nowadays, with the widespread availability of MRI, MS diagnose often largely depends on clinical findings altogether with imaging results (reflecting spatiotemporal dissemination of MS lesions) as well as supplementary CSF-IgG-examination or other additional neurophysiological tests if needed [21]. A quick diagnosis is particularly important for starting early enough disease modifying treatments that can considerably improve the disease's prognosis. Therefore, the development of more sensitive an accurate diagnostic means represents a medical and scientific challenge.

Lesions habitually form around blood vessels and are visualized in vivo by contrast-enhanced MRI, showing leakiness of BBB and white matter pathology, which is commonly used in MS diagnosis to monitor clinical disease progression and therapy response. T2-weighted MRI is used to determine the MS lesion burden, while the common contrast agent used, gadopentetate dimeglumine (Gd-DTPA), also known as gadolinium (Gd), is used to

detect enhancing lesions in T1-weightened images in MS and EAE that correlate with focal inflammation and BBB disruption. However, although MRI with gadolinium-based contrast agents (GBCA) is firmly established as a monitoring tool for MS, a number of discrepancies remain to be approached. Especially in patients with CIS, Gd-enhancing lesions do not always correlate with the clinical scores or the outcome of the disease. This mismatch is denominated the clinico-radiological paradox and is also observed in the murine model of EAE [22], [23]. Given the limited sensitivity of clinical measures for onset and ongoing disease activity, there has been increasing scientific interest in using alternative contrast agent methods to detect and visualize the processes that characterize the initiation of neuroinflammation.

One of these methods extensively researched lately is the application of nanoparticles into the blood stream. Superparamagnetic iron oxide particles have strong magnetic susceptibility effects; thus, their deposition can be visualized by MRI. Studies in humans showed that the application of magnetic nanoparticles in MS patients allows visualization of cellular infiltration in non-Gd-enhancing lesions, giving complementary information on the disparity of MS lesions [24]. Our group has been studying for several years the properties of very small superparamagnetic iron oxyde particles (VSOP) regarding their ability to work as contrast agents in MRI, most importantly to investigate the pathogenesis of MS and EAE and primarily lesion formation. VSOP are nanoparticles that, due to an electrostatically stabilized citrate coating, have a hydrodynamic diameter of only 7 nm, which is importantly smaller than conventional magnetic nanoparticles such as superparamagnetic (SPIO, diameter 150 nm) and ultra-small superparamagnetic (USPIO, diameter 30 nm) iron oxide particles [25],[26].

In contrast to GBCA, iron oxide particles have been shown to be phagocytosed by immune cells and accumulate in liver, spleen and lymph nodes. Hence, they can be used in vivo to monitor macrophages and other mononuclear cells, that play a critical role in the MS inflammatory cascade, whereas Gd only visualizes BBB-leakiness. Altogether, VSOP have the ability to detect inflammatory lesions in early EAE [23], and it might be greater than the results shown by GBCA [27]. As stated before, research has been exploring how to visualize the BCSFB to monitor alterations happening during early inflammation. We showed in previous studies that in EAE, VSOP show early alterations of the CP that take place even before immune cell infiltration into the CNS. When neuroinflammation occurs, VSOP are histologically detected on endothelial structures of the CP, intracellularly in infiltrating myeloid cells, as well as in the perilesional extracellular matrix (ECM) [28]. We could also enlighten how VSOP possibly bind to the CP. In this context, we recently demonstrated that activated brain

endothelial cells could bind to and endocytose VSOP in vitro when exposed to inflammatory stimuli [29].

As an alternative way of monitoring brain barrier breakdown during neuroinflammation, the special properties of VSOP could be used not only in pronounced stages of disease, but also in the beginning, as they are able to visualize subtle but important pathological events, particularly monocyte infiltration, endothelial cell activation, BBB breakdown at lesion sites and CP involvement in BCSFB disruption. Yet, it is unclear, how VSOP behave during different stages of the disease, and which cells are further involved. To better understand the possible uses of VSOP as a means to visualize processes engaged in neuroinflammation, it would be important to identify more cells involved and to understand the behavior of VSOP during relapse and remission. On the other hand, to visualize VSOP within the tissue, iron detection methods have to be applied, which limits the investigation on a histological level. In this work, we studied the behavior of nanoparticles in different stages of EAE, notably regarding their ability to reflect brain barrier breakdown and their colocalization with cells in the CP. Therefore, Europium-doped VSOP (Eu-VSOP) were administered to EAE mice in different stages of the disease. Eu-VSOP can be visualized in fluorescent microscopy and thus show colocalization of VSOP with certain immune cells.

Even if research has been exploring alternative imaging methods to visualize neuroinflammatory events, the question has inadequately been assessed. GBCA not only seem to have limited sensitivity in recognizing subtle changes in early neuroinflammation, but there have also lately been long-term safety concerns. Repeated administrations of GBCA have been associated with progressive and persistent T1 signal hyperintensity in brain tissue of mice and human, most notably the dentate nuclei and the globus pallidus, as a sign of Gd deposits in these regions [30, 31]. Even if the extent of Gd deposits varies between agents, and the clinical impact of this phenomenon remains unclear, the findings raise challenges around GBCA that need to be addressed.

Magnetic resonance elastography (MRE) could represent a promising alternative to the use of GBCA. As a novel imaging technique, it gives information about the mechanical properties of tissues – more concretely about the viscosity, the elasticity and the tissue architecture – by analyzing the tissue's response to oscillatory shear stress. [32]. MRE imaging is already used in clinical diagnostics and evaluation of liver diseases, especially liver fibrosis [33]. Cranial MRE is a novel, non-invasive method of gaining insight in these properties for brain tissue, that can be compared to a virtual palpation, as it is used in the context of clinical examination in other organs.

MRE data includes the G*modulus, that combines the storage modulus G', i.e. the elasticity and the loss modulus G", which reflects the tissue viscosity. If G* – the overall viscoelasticity – decreases, the tissue is experiencing a reduction in the mechanical rigidity, i.e. a "softening". Alterations of tissue architecture or tissue remodelling, as it is common in neuroinflammation, are reflected by changes in the loss tangent ϕ (fig. 3).

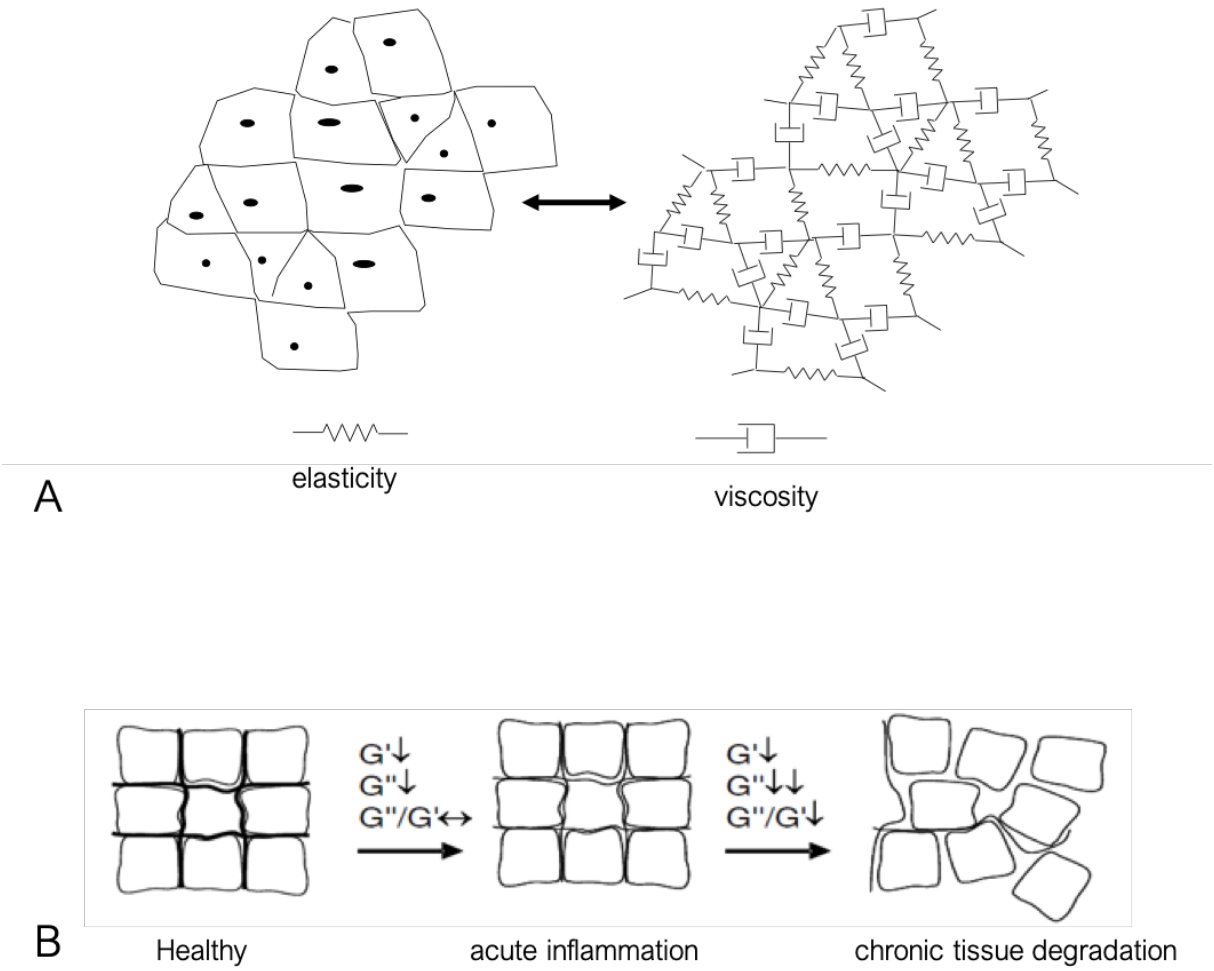

Figure 3. Viscoelastic properties of tissue. A. The storage modulus G'represents the elasticity, the loss modulus G'' the viscosity. B. During acute inflammation, the tissue architecture can stay unaffected, although viscoelasticity may be affected. Only if a reduction of the phase angle (G''/G') occurs, the tissue architecture has been damaged, e.g. during chronic inflammation. Adapted from [34]

In several human studies, researchers have shown viscoelasticity to be a marker for alterations in the brain during normal aging [35] and various neurological pathologies, such as Alzheimers [36], Parkinsons disease [37] or normal pressure hydrocephalus (NPH) [38]. In the context of MS and neuroinflammation, it could present a method of early diagnostic. Using

MRE, our group reported on reduced brain viscoelasticity, i.e. decreased stiffness, in patients with CIS [39]. MS patients show a reduced viscoelasticity compared to healthy controls, both in the relapsing-remitting [40] and in the chronic-progressive forms of the disease [41]. Brain tissue softening was also observed in patients with a neuromyelitis optica spectrum disorder (NMOSD) [42]. In the cuprizone model of MS, which causes rapid demyelination and gliosis when a copper chelator is administered orally in mice, decreased brain stiffness was associated to loss of myelin [43]. Similar results as in MS patients are found in the mouse model of MS, EAE. In mice, the changes in viscoelasticity show a negative correlation with the immune cell infiltration, thus higher T-cell infiltration is correlated with a lower viscoelasticity of the brain, as more inflammation occurs [34]. We further found that elasticity parameters in distinct anatomical regions of the mouse brain differ from each other, the cerebellum being “softer” than the cerebrum [44].

But even if data presenting alterations in viscoelasticity as a marker for neuroinflammation is condensing, prior research has failed to investigate the mechanisms behind these changes. Especially considering the loss of myelin known to be of a fatty and soft consistency, the related loss of stiffness is not intuitive. One would rather expect the tissue to get “harder”, not “softer” during demyelination. When trying to understand the underlying mechanisms that occur during MRE changes, it is crucial to understand what is taken into count in MRE data.

During neuroinflammation, a central aspect in most of the diseases mentioned above, and in EAE, five compartments shape the viscoelastic properties of the brain: neurons, glia, the vasculature, the fluid compartments of the CSF and the ECM. In this work, I leant towards ECM changes to give an explanation for the mechanical alterations, as it seems plausible that a severe tissue remodeling could be engaged in the softening of the brain during EAE.

The CNS ECM is a highly dynamic structure, decisive for the development of neural fibres, providing proinflammatory molecules promoting cell adhesion and differentiation, as well as giving structural plasticity to the tissue [45]. The negative charge of many of its molecules, particularly proteoglycans like fibronectin, and its three-dimensional ultrastructure influence normal CNS tissue development. In embryology, some molecules have been shown to be involved in neurite outgrowth and axonal guidance [46, 47] and oligodendrocyte differentiation [48].

In neuroinflammation, especially in terms of disease progression, alterations of ECM developing in the course of MS are ambiguous. BBB breakdown, release and activation of extracellular proteases and proinflammatory cytokines collectively induce ECM-depositions of collagens, proteoglycans (PGs) and chondroitinsulfate proteoglycans (CSPGs) in early active

lesions. In chronic lesions as well as the NAWM these ECM deposits can inhibit remyelination [49, 50]. Many PGs and CSPG, such as fibronectin, versican, aggrecan, neurocan, inhibit the differentiation of OPCs and thus the reparation of tissue [51, 52]. But interestingly, numerous scientific findings suggest an inconclusive action of some molecules. ECM components such as collagens, biglycan and decorin, may also interfere with immune and glial cells to form a perilesional scar limiting the enlargement of MS lesions [53]. In particular, the differential spatiotemporal expression of ECM PGs could be one important influence on remyelination [54]. Especially laminins seem to be permissive for remyelination by guiding the proliferation, survival and maturation of oligodendrocyte lineage cells [55, 56]. However, supplementary to the substantial and perceptible alterations that are seen in MRI and histological MS lesions, there seem to be more subtle and widespread abnormalities contributing to axonal damage in the ECM of normal-appearing white matter (NAWM) [57].

Aims

In the course of this study and considering the findings mentioned above, I aimed to explore alternative visualization techniques and novel MR-based imaging methods of brain barrier breakdown as a central step for initiation and maintenance of neuroinflammation in the relapsing-remitting model of EAE. In the context of two complementary experimental projects I investigated:

1. The suitability of Europium-doped nanoparticles to monitor in vivo and ex vivo BCSFB and BBB alterations
2. The visualization and assessment of remodeling at BBB sites during inflammatory events by MRE

Methods

Experimental set-ups

This research plan was conducted in three different blocks of experiments, that were established as follows. Experimental procedures are further outlined hereafter.

The first block, which was implemented in collaboration with Millward et al. and published by our group in 2017 [58], explored the potential of Eu-VSOP to visualize central elements of neuroinflammation, such as BCSFB breakdown and EAE lesions. For the experimental set-up, 18 SJL mice were immunized with PLP and CFA and pertussis toxin to induce a RR-EAE. Mice were separated in two groups and scanned at different timepoints of disease: In the first group (n=8) MRI was performed on day 14 post immunization (p.i.), a timepoint were mice normally reach the peak of clinical impairment, in the second group (n=10) MRI images were acquired at day 21 (remission) and day 28 (relapse). Eu-VSOP were applied each timer after MRI scans and post-contrast MRI was performed 24 hours later. Mice were sacrificed after the final scan, for histology (fig. 4).

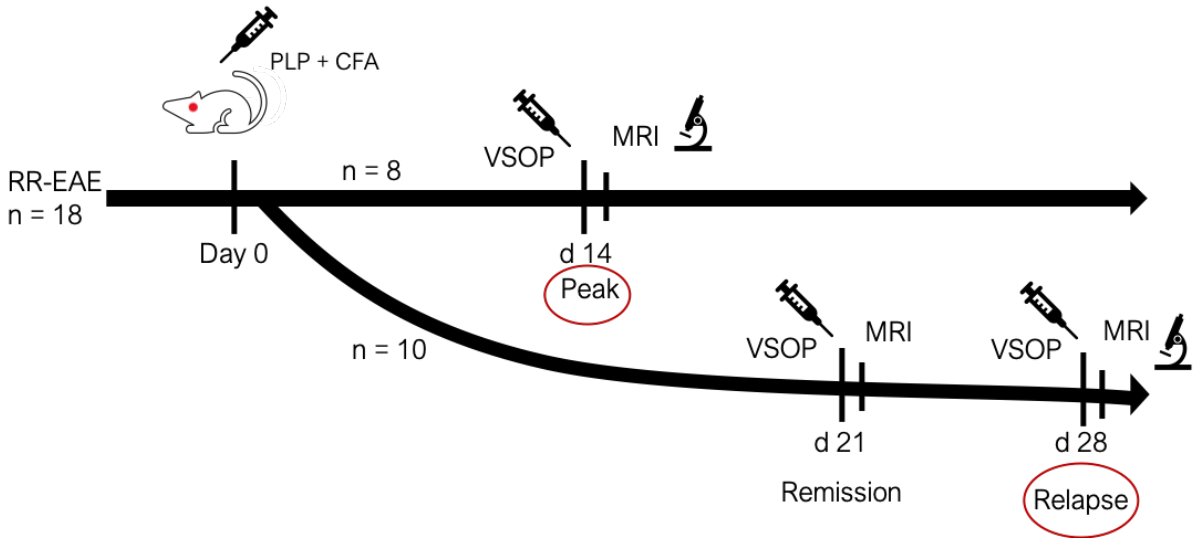

Figure 4. Experimental set-up for Eu-VSOP.

The second block of analyses was performed in collaboration with S. Wang, J.M. Millward et al. and is currently in process of publication. It applied MRE to monitor mechanical alterations as a manifestation of BBB disruption. Over multiple experiments, mice were divided in two groups: EAE mice (n=25) and non-manipulated healthy controls (n=7). 25 SJL mice were immunized as explained below to develop an active EAE and MRE brain scans were performed at peak disease. The following day, mice received a GBCA-enhanced MRI of the brain. Mice were subsequently sacrificed for RT-PCR and histology (fig. 5).

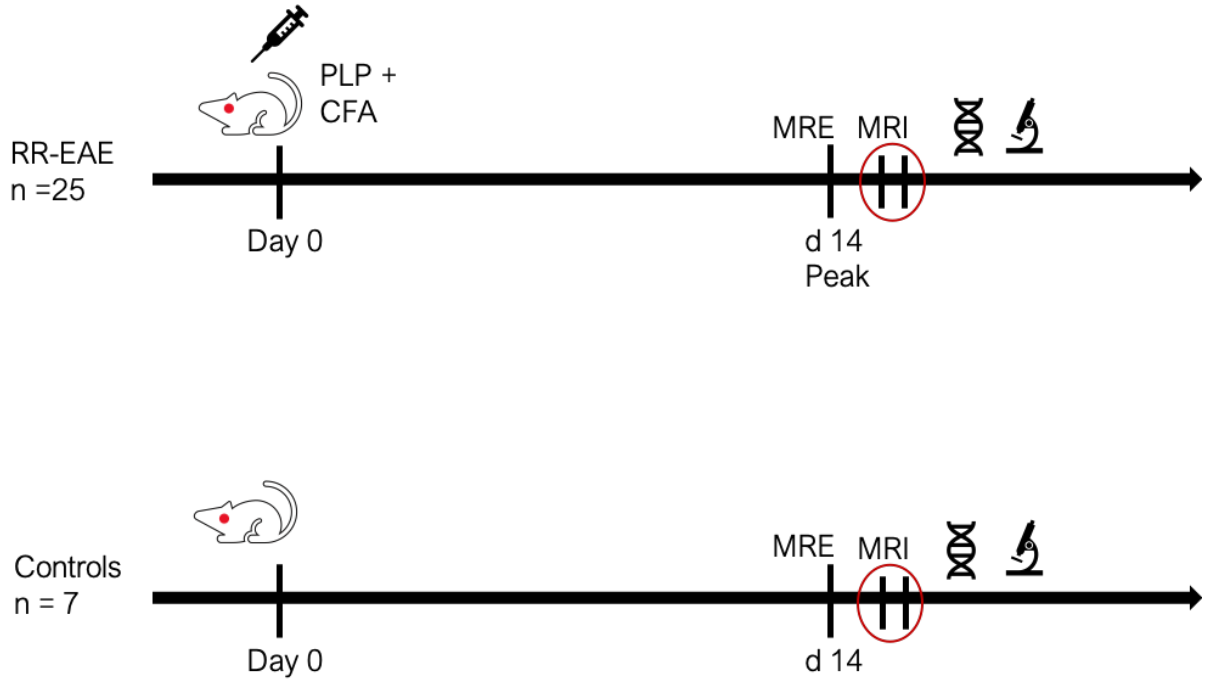

Figure 5. Experimental set-up for MRE. S. Wang, J.M. Millward, L. Hanke-Vela et al.

In the third block, to further investigate histological findings over different timepoints of EAE, we induced EAE on 9 SJL mice to analyze the Fn expression in EAE tissues over time. EAE-mice were immunized on day 0 and developed a RR-EAE by day 10 p.i. 4 mice served as controls, from which 3 were immunized with CFA only and one remained completely unmanipulated. At day 14, and day 25, i.e. at peak and remission phase respectively, mice were sacrificed, and tissues processed for histology as explained underneath (fig. 6).

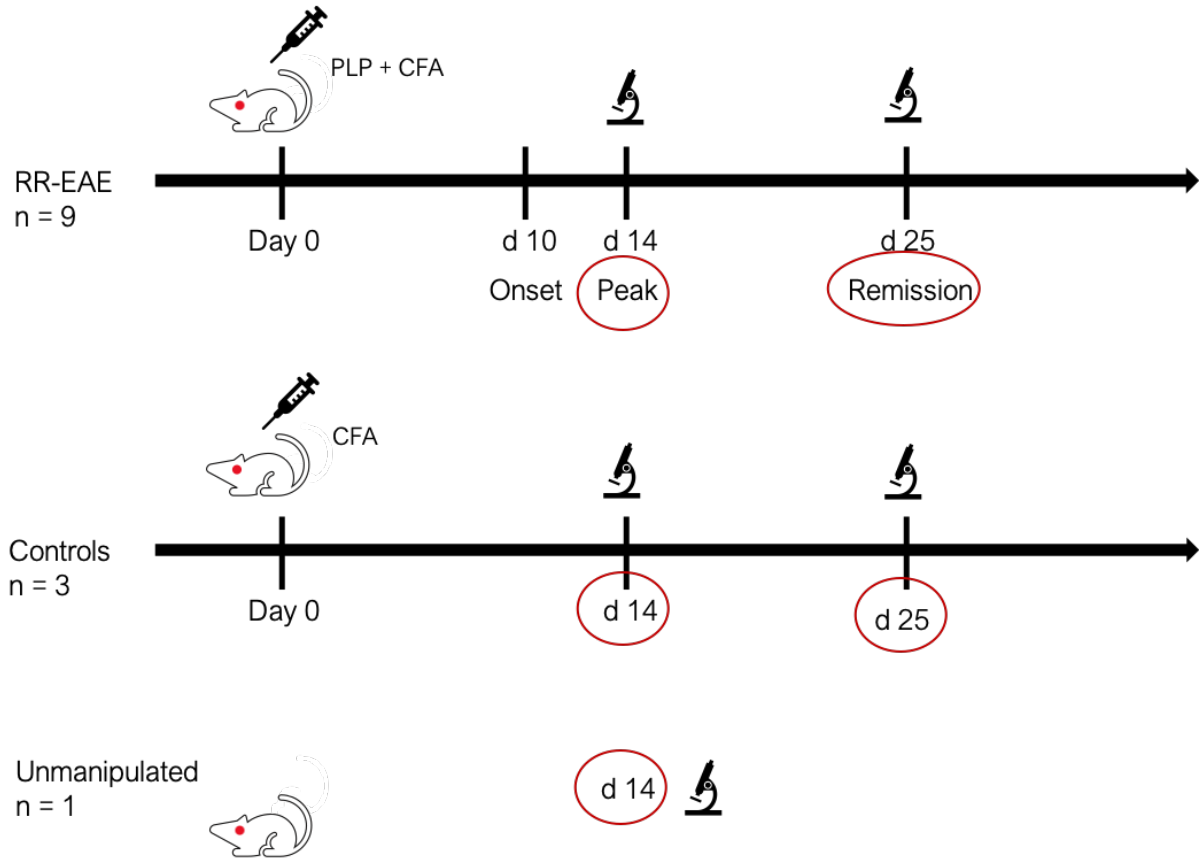

Figure 6. Experimental set-up for Fn stainings at peak and remission.

Animals

All procedures were approved by the local animal welfare committee (Landesamt für Gesundheit und Soziales, LaGeSo Berlin) in accordance with national and international guidelines to minimize discomfort to animals (86/609/EEC). Experimental Swiss Jim Lambert (SJL) mice were purchased from Janvier and were housed in the central animal facility of the Charité – Universitätsmedizin Berlin Virchow Klinikum. All animals were kept in a temperature- and humidity-controlled colony room and maintained on a light/dark cycle of 12/12h with ad libitum access to food and water.

Active EAE

To induce active EAE, SJL mice were immunized subcutaneously with 250 µg PLP peptide 139-151 (purity 95%; Pepceuticals, Leicester, UK) and 800ug Mycobacterium tuberculosis H37Ra (Difco, Franklin Lakes, NJ, USA) emulsified in 100 µl Complete Freund's adjuvant (CFA) and 100 µl phosphate-buffered saline (PBS). Immunization was administered subcutaneously (s.c.) on the back and tail base. Pertussis toxin (250 ng per mouse; List, Biological Laboratories, Campbell, CA, USA) in 200µl PBS was injected intraperitoneally

twice, on the day of immunization (day 0) and again 2 days later (day 2). After immunization, mice were monitored daily for clinical signs of EAE and scored as follows: 0, no disease; 1, tail paralysis; 2, paralysis; 3, paraplegia; 4, paraplegia with forelimb weakness or paralysis; 5, moribund or dead animals (details see table 1). Control mice were immunized with CFA only or left completely unmanipulated.

0,25	(TPA)
0,5	TPA
0,75	TPA-L
1,0	TPL / TPA + RRW
1,25	TPA-L + RRW
1,5	TPL + RRW
1,75	(HPA) + TPA/ TPL/ RRW
2,0	HPA + TPA/ TPL/ RRW
2,5	HPA –L + TPA/ TPL/ RRW
3,0	HPL + TPA/ TPL/ RRW
4,0	FPA + TPL + HPL
4,5	Moribund FPL + TPL + HPL
5	Day after death

Table 1. Detailed clinical score of EAE mice. TPA = Tail paresis. TPL = Tail plegia, RRW = Righting Reflex weak, tried 5x into one direction, HPA = Hind limb paresis, HPL = Hind limb plegia, FPA = Fore limb paresis, FPL = Fore limb plegia.

Europium-doped very small superparamagnetic iron oxide particles

Europium-doped very small superparamagnetic iron oxide particles (Eu-VSOP) were produced exclusively by the Charité Department of Radiology in the nanoparticle working group. For synthesis of these nanoparticles, a fraction of Fe^{3+} in a weight ratio of 5% was replaced by Eu^{3+}. For that, different amounts of europium(III) chloride hexahydrate (Sigma-Aldrich, USA) were added to synthesized VSOP (0.236 g for Eu-VSOP-1; 0475 g for Eu-VSOP-2; 0.706 g for Eu-VSOP-3; 0.880 g for Eu-VSOP-4; 1.185 g for Eu-VSOP-5; 1.77 g for Eu-VSOP-6; and 2.37 g for Eu-VSOP-7). The europium chloride can only be dissolved after the iron(III) chloride has been dissolved to assure sample homogeneity. Once the europium(III) chloride has entirely dissolved, the iron(II) chloride is added. Preparation batch was Eu-VSOP-7, with an iron concentration of 0.122 mol/L and Europium concentration of 0.00123 mol/L. Detailed information on the chemical synthesis and characterization of the particles has been published

previously [59, 60]. Eu-VSOP detection using fluorescence microscopy was conducted using a customized enhancer solution (Eu-enhancer, HEE), based on the antenna system used with the commercially available DELFIA® Enhancement solution (Perkin Elmer) and developed by Ariza de Schellenberger et al. at the Department of Radiology [61]. Images were obtained in an Axio Observer.Z1 with AxioVision Software ZEN 2012 (Carl Zeiss AG. Oberkochen, Germany). Europium was detected with a customized filter set consisting of an excitation filter (BP 350/50 nm), a beam splitter filter (380 nm LP), and an emission filter (HC 615/20 nm) (AHF Analysentechnik AG, Tübingen, Germany). [60]

bEnd.3 cells

Murine brain vascular endothelial cells from cell line bEnd.3 were obtained from ATCC. Cells were cultured in Dulbecco's modified Eagle's medium (DMEM) supplemented with 10% fetal calf serum (FCS) at 37°C with 5% CO_2, on 12 mm glass cover slips in 6-well plates at a density of 105 cells per well. The cells were incubated in serum- free medium for 24 h before 0.1mM Eu-VSOP were added for 4h, with or without stimulation using 10ng/ml tumor necrosis factor alpha (TNFα). Following, the cells were washed with PBS, and fixed for 10 min with 1:1 acetone–methanol, pre-cooled at -20 °C, and then processed for staining with the HEE solution for 10 min.

MR imaging for Eu-VSOP detection

MR in vivo scans were collected on a 7 T Bruker Pharmascan 70/16 rodent MR scanner (Bruker Biospin, Ettlingen, Germany), with a 20 mm RF Quadrature-Volume head coil (18–20). Mice were anaesthetized with 1.5–2.0% isoflurane in 30% O_2 and 70% N_2O administered via face mask, under continuous ventilation monitoring (Bio Trig System, Bruker Biospin) (21). The animals were placed on a bed with circulating heated water to maintain constant body temperature at 37°C.

T2*-weighted images were acquired with the following parameters: axial – (FLASH, TE 7.2 ms, TR 619.7 ms, flip angle 30°, 0.44 mm slice thickness, matrix 256, FOV 2.85 cm, 4 averages, 40 slices, scan time 10 min 34 s); coronal – FLASH, TE 7.2 ms, TR 386.2 ms, flip angle 30°, 0.43 mm slice thickness, matrix 256, FOV 2.85 cm, 4 averages, 25 slices, scan time 6 min 35 s.

T1-weighted images were acquired 5 min after animals received intravenous (i.v.) 0.2 mmol/kg Gd- DTPA (Magnevist, Bayer-Schering AG). Data acquisition was done with ParaVision 5.0 (Bruker Biospin, Germany).

Two groups of animals were scanned independently. Scans in the first group (n=8) were performed at day 12-14 p.i., at peak disease. Animals in the second group were imaged during remission and relapse, corresponding to day 21 and 28 p.i. respectively. After baseline pre-contrast images were acquired, animals received 0.2 mmol/kg of Eu-VSOP i.v. and stayed in the home cage until post-contrast images were acquired 24 h later. This timespan allows the nanoparticles to be eliminated from the blood pool. The dose and timing were established in our previous studies using VSOP in EAE [23, 27, 28].

In vivo scans for MRE

In vivo MRE and MRI scans were performed as described previously [44] on a 7 T Bruker Pharmascan 70/16 rodent MR scanner (Bruker Biospin, Ettlingen, Germany), with a 20 mm RF quadrature volume head coil (RAPID Biomedical GmbH, Rimpar, Germany). Mice were anaesthetized and monitored for respiration and body temperature as explained above. Data acquisition was done with Paravision 5.1 software. In those animals investigated by both MRE and MRI, the MRE measurements were acquired first, followed by GBCA-MRI after 24h.

Magnetic Resonance Elastography

MRE data was acquired in one 2 mm midsagittal slice as described in our previous work [44]. Mechanical vibration was generated by an air-cooled electromagnetic Lorentz coil triggered by the MRI scanner and transferred to the animal through a carbon fiber piston, which was connected to the bite bar transducer. The transducer was gimbaled through a rubber bearing and retaining bracket at the temperature-controlled mouse bed. A plastic disk held up the entire setup in the center of the magnet bore.

The timing of the vibration was defined and recorded by a fast low-angle shot (FLASH) sequence especially made for MRE measurement. The direction of the motion sensitizing gradient (MSG), with a strength of 285 mT/m, a frequency of 900 Hz, and 9 periods, was maintained parallel to the principal axis of the magnetic field. To compensate for the static phase contributions, phase difference images were calculated from two images differing in the sign of the MSG. Frequency amplitude and the number of cycles were controlled by a waveform generator connected via an audio amplifier to the driving coil. Additional scan parameters were as follows: TE = 14.3 ms; TR array = 166.0 ms; slice thickness = 1.0 mm; matrix = 128, FOV

= 25 mm; two averages; eight dynamic scans over a vibration period and an acquisition time of 12 min.

MRE data analysis

Complex wave images corresponding to the harmonic drive frequency were extracted by temporal Fourier transformation of the unwrapped phase-difference images. To reduce noise, in addition to the Butterworth band pass filter, a spatiotemporal directional filter was applied to the wave images, as waves were observed propagating predominantly bottom-to-top in the sagittal slice. A 2D-Helmholtz inversion was performed to the filtered data, yielding the complex shear modulus G* and the magnitude modulus |G*| = abs (G*). The tabulated spatially averaged G*-values were represented by the real part of the complex shear modulus G′ = Re (G*), known as the storage modulus that represents tissue elasticity, and the imaginary part G″ = Im (G*), which is the loss modulus representing tissue viscosity. The magnitude, storage and loss moduli were expressed in pascals (Pa). The loss factor calculated as the phase angle φ = atan (G’’/ G′) represents the degree of viscosity relative to elasticity and is interpreted as being sensitive to the architecture of viscoelastic networks in biological tissues [62]. In addition to calculating values for the storage and loss moduli for the entire sagittal slice, the brain was separated into two regions of interest (ROI) divided at the junction between the cerebrum and the cerebellum.

MRI in MRE experiment

T1 maps were generated using a saturation recovery RAREVTR method, in which the repetition time (TR) was varied to acquire a series of axial T1 weighted images, from which the T1 map was produced. Scan parameters were as follows: TE = 8.3 ms; TR array = 230, 460, 1061, 1485, 2080, 3080 and 7500 ms; flip angle = 90°/180°; RARE factor = 2; slice thickness = 1.0 mm; matrix = 128, FOV = 1.92 cm; NA = 1, 10 slices, scan time = 17 min 44 sec. After acquiring the pre-contrast T1 map, the animals were administered 0.2 mmol/kg Gd-DTPA (Magnevist, Bayer Vital GmbH, Leverkusen, Germany) by intravenous injection. After 5 min, the post-contrast T1 maps were acquired using the same parameters as above. Data acquisition was done with ParaVision 5.1 (Bruker Biospin, Germany). The raw data files were exported as NIFTI image files, and analyzed in ImageJ v. 1.51 (NIH, open source). A region of interest (ROI) defining the brain was manually traced for all 10 slices, and the mean T1 value of each ROI calculated. The mean T1 from all 10 slices was determined for each animal, and the post-

contrast mean was subtracted from the pre-contrast mean, to yield the difference – Δ T1. The Δ T1 was used for the statistical analysis.

T1-weigthed images were acquired as described in our previous papers: axial T1w images (RARE, TE 10.5 ms, TR 804.1 ms, 0.5 mm slice thickness, matrix 256, FOV (field of view) 2.85 cm, four averages, 30 slices, scan time 6 min 51 s); coronal T1w images (RARE, TE 10.6 ms, TR 938.1 ms, 0.5 mm slice thickness, matrix 256, FOV 2.85 cm, four averages, 25 slices, scan time 8 min 32 s) [28]. As a complimentary method, we also calculated the T1 signal intensity (SI) change directly from the T1-weighted images. An ROI defining the brain was manually traced for 20 slices and the mean SI value of each ROI was calculated. The mean SI from all 20 slices was determined for each animal in both pre- and post-contrast, calculated as: signal intensity change (SI%) = (SI post-contrast – SI pre-contrast) / SI pre-contrast * 100).

Tissue processing

After terminal anesthesia with ketamine, mice were transcardially perfused with 20 ml PBS to rinse erythrocytes out of blood vessels. Brains and lymph nodes were extracted, and post-fixed in zinc fixation solution (0.5% zinc acetate, 0.5% zinc chloride, 0.05% calcium acetate) for at least 3 d at room temperature. Tissues were then processed for routine dehydration and paraffin embedding, and 5 µm sections cut with a microtome. An alternative fixation in PFA and consecutive freezing was chosen for experiments concerning ECM stainings. A sucrose protection (30% sucrose in PBS) was applied before tissue freezing: brains were soaked into solution until sinking to the bottom, generally after one day. Brains were cut in 3 portions coronally (forebrain, midbrain, cerebellum) and placed with the anterior part (except for forebrains) on a small labeled cryo mould. Forms were placed swimming in methyl butane cooled down with dry ice to -75°C and frozen in tissue tek O.C.T. (Optimal Cutting Temperature) (Sakura Finetek, Alphen aan den Rijn, NL, Europe), then stored at -80°C.

Serial coronal sections of paraffine embedded brains were generated on a Leica Microtome SM2010R with a thickness of 5 µm. To visualize CP, it was taken care of cutting in a plane with good view on the ventricular system in the midbrain.

Serial coronal sections of frozen tissues were generated on a Leica cryostat CM3050S with a thickness of 12 µm.

Haematoxylin and eosin (H&E) stain for morphological overview

Paraffine slides where previously deparaffinized and rehydrated using a descending Neo-Clear solution (Merck, Darmstadt, Germany). Frozen sections where thawed at room temperature for

30 minutes. Sections where incubated with 4% PFA (paraformaldehyde) for 10 minutes and shortly rinsed in aqua dest. Sections where then immersed in haematoxylin solution for 10 minutes and washed in flowing tap water for 2 minutes. After a short rinse in aqua dest. After an incubation of 45 sec. in eosin solution, sections where briefly dunked in tap water and subsequently dehydrated in an ascending ethanol solution (70%, 80%, 95%, 2 x 100%) and Neo-Clear. Sections where embedded with Neo-Mount solution (Merck, Darmstadt, Germany).

Brain lesion distribution

Sections were analyzed under an Olympus BX40 microscope. To evaluate inflammation and EAE lesions in distinct regions, a template was filled out for every mouse and H&E section. ROI evaluated were, in the midbrain: ventricles, thalamus, hippocampus, cortex, meninges. In the cerebellum: cerebellar white matter, cerebellar grey matter, brainstem, meninges. Forebrain sections were not quantified, as the SJL-EAE is known to mostly affect midbrain and cerebellum.

Prussian blue intensification with DAB for VSOP detection

Sections where deparaffinized or thawed as explained before. 2 % Potassium ferricyanide was applied for 5 min, then 6N HCl added in a concentration of 50 µl/ml added for 5-20 min. Sections were then washed twice for 5 min in aqua dest. 3,3'-Diaminobenzidine (DAB) intensification was applied in a solution of 0,05% in PBS (pH 7,4) and 0,03% H_2O_2 for several minutes. Sections were checked microscopically for the desired intensity and then washed in aqua dest. Counterstaining was performed with Nuclear Fast Red (Sigma).

Fluorescence microscopy for Eu-VSOP detection

For fluorescent detection of Eu-VSOP, tissues or cells were incubated with the HEE customized fluorescent enhancer solution. Enhancement solution was applied for 10 min in the dark at room temperature, air dried for 5 min, then mounted with Fluoromount (Sigma). The fluorescent signal was left to intensify for 1 h, then images were acquired using a Zeiss Axio Observer microscope, with a filter set allowing for excitation of 350 nm and emission of 615 nm. For combined immunofluorescence and Eu-VSOP detection, the immunostaining protocol was done first, followed by application of the enhancement solution.

Immunofluorescence stainings

For Eu-VSOP experiment, frozen sections were thawed at room temperature and dried completely before proceeding. Paraffine embedded tissues were rehydrated as mentioned before. Each slide presented 2 serial sections, which were outlined individually using a DAKO pen (Dako Denkmark A/S). Sections were incubated with 4% paraformaldehyde (PFA) for 10 minutes at room temperature and rinsed with PBS. An avidin- and biotin-blocking solution was applied consecutively for 15 minutes each. After rinsing with PBS, a protein blocking solution (1% bovine serum albumine + 10 % normal goat serum, 0.1% Triton-X for permeabilisation) was applied for 1h at room temperature. Excess protein block was removed without rinsing the slide, and sections where then incubated with primary antibody: monoclonal biotinilated rat anti-mouse F4/80-biotin (Biolegend), diluted 1:200 in PBS or with 1:100 FITC-conjugated anti-mouse pan-cytokeratin (Sigma) overnight at 4°C. The next day, F4/80 staining was completed by rinsing sections with PBS and incubating with streptavidin-PE-Cy5 (1:500).

Fixed bEnd.3 cells were stained with 1:2000 mouse anti-claudin-5 (Invitrogen), followed by 1:500 AF488-conjugated goat anti-mouse IgG (Invitrogen).

Fibronectin (Fn) immunostaining

Sections were deparaffinized and rehydrated as explained before. One slide presented 3 serial sections, one of which was used as negative control. Slides were incubated in 4% PFA for 10 minutes and rinsed in PBS. Sections were individually outlined with a DAKO pen. Brain sections were permeabilized and blocked with PBS containing 10% normal goat serum, 10% bovine serum albumin and 0.3% Triton TM X-100 for one hour at room temperature. Sections were then incubated in first antibody, including: rabbit anti-mouse Fn diluted in blocking solution 1:250 (Millipore ab2033); mouse anti-EIIIA-Fn, 1:200 (Abcam ab6328); chicken anti-GFAP, 1:500 (Abcam ab4674) overnight at 4°C. For double labelling immunostaining, primary antibodies were incubated sequentially. For staining with the mouse anti-EIIIA-Fn (IST9), we used a mouse on mouse (M.O.M.) kit from Vector Laboratories. After rinsing in PBS, the secondary antibody was applied: goat anti-rabbit Alexa Fluor 488 or 647, 597, (1:400) at room temperature for 2 hours. After rinsing, Sections were counterstained with 4′,6-diamidino-2-phenylindole (DAPI) for visualization of nuclei (1:10.000) for 2 minutes, then rinsed and mounted with cover slide and Immunomount.

Sections were imaged using a Zeiss Axio Observer fluorescence microscope, a laser-scanned confocal microscope (LSM 710, Carl Zeiss, Jena, Germany) or an Operetta High Content Imaging System (Perkin Elmer).

Quantitative reverse-transcription polymerase chain reaction (RT-PCR

The brain tissue for PCR was divided into two portions, the anterior (cerebral) and posterior (cerebellar) region, according to the MRE scanning regions. Total RNA was extracted from the tissue by using the Trizol method. The RNA was reverse-transcribed, using Moloney murine leukemia virus reverse transcriptase (Invitrogen Life Technologies) with random hexamer primers. Quantitative PCR (qPCR) was then performed with 1 µl of cDNA sample in a 25-µl reaction volume containing 12.5 µl of TaqMan PCR Master mix (Applied Biosystems), forward and reverse primers (900nM), and TaqMan probe (200 nM; Applied Biosystems). We used an ABI Prism 7000 SequenceDetection System (Applied Biosystems, Darmstadt, Germany). Quantitative real-time PCR was confirmed on cerebellum of mice at day 14 and 28, with tissue of a previous EAE experiment on SJL mice [34] and performed as described before. Primers and probes were from Eurofins MWG Operon (Ebersberg, Germany), and the sequences used are as followed: Fibronectin, forward *5'-ATCATTTCATGCCAACCAGTT-3'*, reverse *5'-TCGCACTGGTAGAAGTTCCA-3'*, probe *5'FAM-CCGACGAAGAGCCCTTACAGTTCCA-3'*TAMRA. Neurocan, forward *5'-GGTGTGCGCACTGTGTA-3'*, reverse *5'-CATGTTGTGCTGTATGGTGATG-3'*, probe *5'FAM-TTCGACGCCTACTGCTTCCGAG-3'*TAMRA. Brevican, forward *5'-AGAACCGCTTCAATGTCTACTG-3'*, reverse *5'-ACTGTGACAATGGCCTCAAG-3'*, probe *5'FAM-ACTCTGCCCATCCCTCTGCTTC-3'*TAMRA. Glypican5, forward *5'-GAGACACTTGCCAACAGAAGA-3'*, reverse *5'-GGGCAGCCAATTCATTAACAC-3'*, probe *5'FAM-CATGGGTCCTTCTATGGTGGCCTG-3'*TAMRA. 18s, served as the endogenous reference, forward *5'-TTCGAACGTCTGCCCTATCAA-3'*, reverse *5'-TCCCCGTCACCCATGGT-3'*, probe *5'FAM-TGATGTTTATTGACAACACGCTTTACTTTATACCTGAAGA-3'*TAMRA. CD3epsilon: forward 5′-CCT CCT AGC TGT TGG CAC TTG-3′, reverse 5′-CAC TGG TTC CTG AGA TGG AGA CT-3′, probe 5′FAM-CAG GAC GAT GCC GAG AAC ATT GAA TAC A-3′TAMRA. Lung tissue served as a positive control for Fn expression. Cycle threshold values were converted to arbitrary units using a standard curve, and data are reported as the ratio of target gene expression over 18s rRNA, which served as the endogenous reference. We used the $2^{-\Delta\Delta C_T}$ method to analyze the results.

Statistical Analysis

Data were analyzed by unpaired two-tailed t-test, paired two-tailed t-test or repeated-measures analysis of variance (ANOVA), as appropriate. To assess the correlation between MRE parameters and EAE score, a non-parametric Spearman correlation was used. The Pearson

correlation was calculated to assess the correlation between imaging parameters, and between MRE parameters and the PCR. Analysis was done using GraphPad Prism v.5.01. (GraphPad software, La Jolla, CA, USA). * $p < 0.05$, ** $p < 0.01$, *** $p < 0.001$.

Results

I. Monitoring alterations of BCSFB and BBB with EU-VSOP

Our group has previously worked on finding alternative imaging methods to visualize alterations linked to neuroinflammatory processes. As stated in the introduction, one central pathophysiological mechanism in the initiation of EAE and MS is the breakdown of CNS barriers, such as the BCSFB within the CP. As a floating complex inside of the ventricles, the CP serves as an interface between blood pool and the CSF, but its slim structure makes it impossible to visualize early alterations with conventional contrast agents like gadolinium. Our group has previously shown that VSOP are able to visualize BCSFB malfunction in early stages of EAE, before even immune cell infiltration occurs [28]. In this work, we used Eu-VSOP to visualize BCSFB-breakdown and EAE lesions in vivo and in fluorescence microscopy, in order to further enlighten the histological processes of this important pathophysiological step.

The following results were found in collaboration with Millward et al. and published in the paper entitled "Application of Europium-Doped Very Small Iron Oxide Nanoparticles to Visualize Neuroinflammation with MRI and Fluorescence Microscopy". Neuroscience, 2017 [58].

Fluorescent imaging visualizes inflammation-induced uptake of Eu-VSOP by brain endothelial cells

Our group showed recently, that murine brain endothelial cells could efficiently uptake VSOP and that in vitro, inflammatory stimuli increased VSOP uptake by bEnd.3 cells, an endothelial cell line of the BBB [29]. In the present work, in order to confirm that Eu-VSOP display the same characteristics as non-Eu-VSOP, we applied identical conditions to the bEnd.3 cells as in our previous study. In cell culture, Eu-VSOP were spontaneously taken up by unstimulated bEnd.3 cells (Fig. 7 A, B), and, in analogy to our previous observations with VSOP and Prussian blue staining, accumulated in the cytoplasm and perinuclear. As in our previous study, stimulation of bEnd.3 cells with 10 ng/ml TNFα provoked an increased uptake of Eu-VSOP (Fig. 7 C, D). We then combined the fluorescent detection of Eu-VSOP (Fig. 7 E) with immunofluorescent staining for claudin-5, a marker for tight junctions in brain endothelial cells (Fig. 7 F). Fluorescent imaging identified the definite intracellular, cytoplasmic location of the nanoparticles within the bEnd.3 cells and confirmed the compatibility of Eu-VSOP with immunostaining.

In our experiment, Eu-VSOP were taken up by brain endothelial cells and this process was enhanced under inflammatory stimuli.

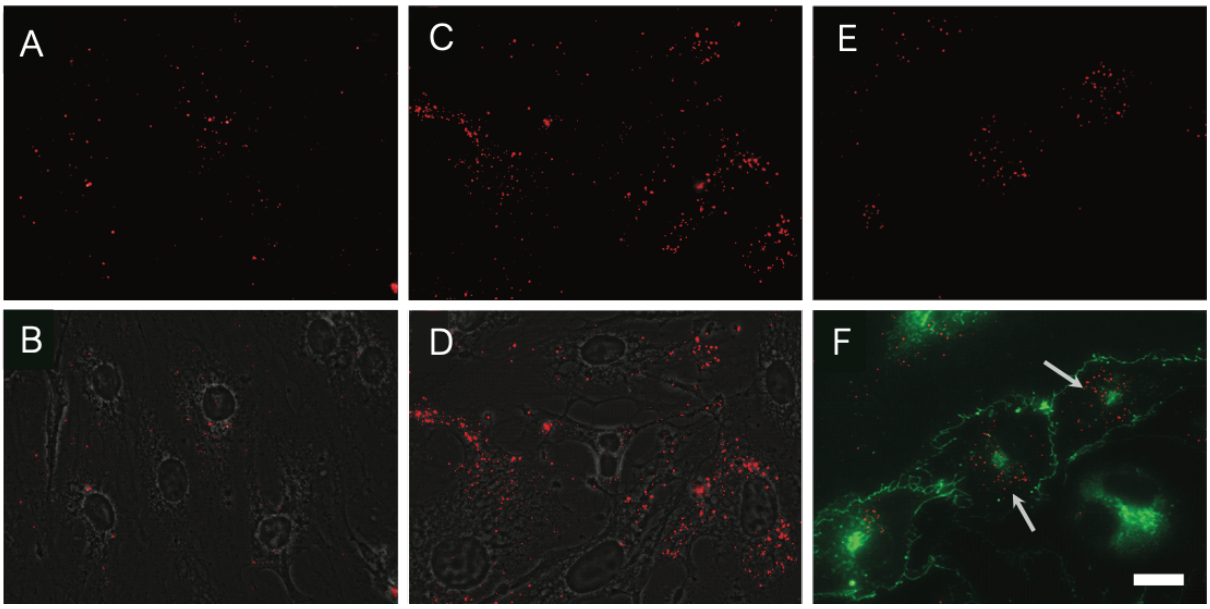

Figure 7. Eu-VSOP uptake by bEnd.3 cells. (A, B): Endothelial cells bEnd.3 spontaneously uptake Eu-VSOP (red). (C, D): Uptake is increased under stimulation with TNFα. Fluorescent detection of Eu- VSOP (A, C) overlaid with phase contrast images (B, D).(E): Fluorescent microscopy of Eu-VSOP and immunofluorescent staining for claudin-5 – tight junctions (green, F) in bEnd.3 cells show definite cytoplasmic location of the nanoparticles (arrows) (F). Scale bar = 20 µm. [58]

Monitoring EAE lesions and BCSFB alterations in vivo at peak EAE

To investigate the ability of Eu-doped VSOP to identify EAE lesions in vivo, we administered Eu-VSOP in EAE mice. SJL mice were immunized with PLP and developed clinical signs of a RR-EAE around 9-10 days p.i. Peak disease was identified by clinical severity scores and was reached normally between 12-14 days p.i. Our group then acquired T2*-weighted pre-contrast images on a 7T rodent MRI scanner. After collection of these baseline-images, Eu-VSOP were administered i.v. and post-contrast images were collected 24 hours later. This timespan had been determined in previous studies for VSOP [23, 27, 28], as by 24 hours the nanoparticles have been washed out of the blood pool, leaving pathological accumulations for detection by MRI.

At the timepoint of the MRI scans, all sick animals showed pathological accumulation of Eu-VSOP in forebrain, midbrain and cerebellum. Lesions in MR images had a hypointense, focal punctate appearance and were comparable between different mice in shape, size and distribution over brain regions. Images of a representative mouse are shown in figure 8 (upper set of images). Eu-VSOP accumulations in the ventricles highlighted the involvement of the

CP in the peak phase of EAE. Moreover, lesions containing Eu-VSOP had the same appearance as lesions identified by VSOP without Europium, if compared with images of our previous study in SJL mice (Fig. 8, middle set). We further compared Eu-VSOP imaging to Gd-contrast agents. Therefore, separate EAE mice underwent a standard imaging procedure: Gd-DTPA was injected in a dose of 0.2mmol/kg 5 min prior to collection of MR images. Typical for EAE lesions, the T1 weighted images showed a diffuse hyperintense appearance (Fig. 8 bottom set).

In vivo MRI scans in EAE mice at peak disease with Eu-VSOP showed the ability of these nanoparticles to visualize lesion formation in forebrain, midbrain, cerebellum and ventricles, where the nanoparticles demonstrate alterations of the BCSFB and the involvement of the CP. The appearance of EAE lesions was comparable to those seen with VSOP in prior studies.

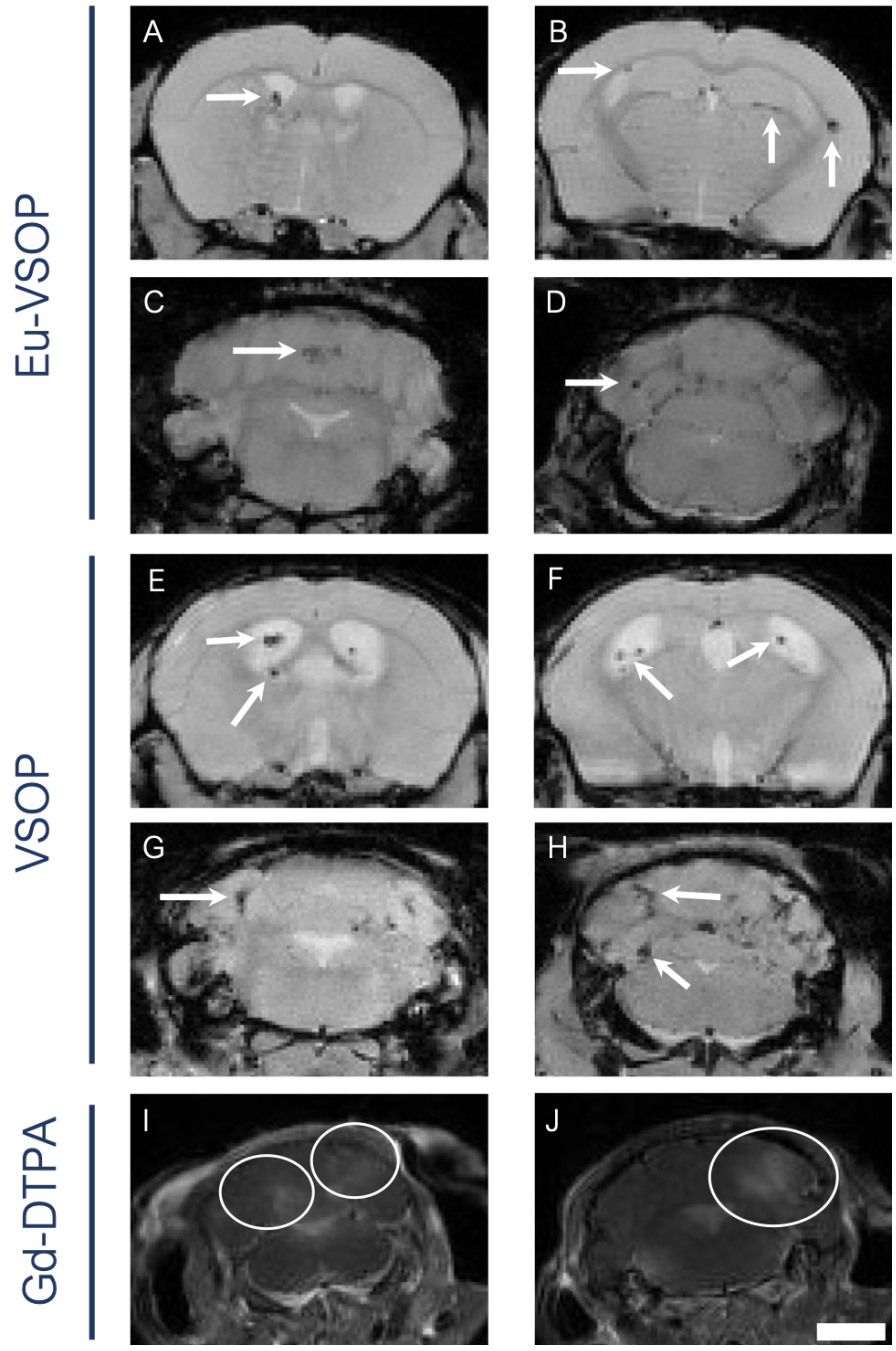

Figure 8. In vivo detection of inflammatory lesions at peak disease of RR-EAE. T2 weighted coronal images of mouse brains. Focal Eu-VSOP accumulations are seen as punctual hypointensities throughout the cerebrum (arrows in A,B) and cerebellum (C,D). Equivalent signal extinctions from VSOP accumulations in a different animal are shown in E–H. Images show Eu-VSOP and VSOP accumulations in gray matter, white matter, ventricles and interventricular foramen. T1- weighted images show typical diffuse hyperintense gadolinium-enhancing lesions in a separate animal (circles in I-J). Scale bar = 2 mm. [58]*

Eu-VSOP to monitor remission and relapse phases

In previous studies using VSOP we focused primarily on peak and pre-onset phases of the disease. Here, we used the SJL EAE model, that is widely used to analyze remission and relapse phases, to explore how reliable the Eu-VSOP-based MRI is during the relapsing-remitting disease course and especially in advanced EAE pathology. Therefore, mice were scanned one

day after Eu-VSOP administration during remission phase (day 21 p.i.). Figure 9 shows a representative example of a mouse that presented severe clinical impairment at peak disease, of which the clinical score had decreased to 0 by day 21 p.i. Representative examples of T2*-weighted coronal and axial MR slides show no hypointensities as caused by Eu-VSOP lesions in remission phase. From the animals that had shown clinical signs at peak disease and that were scanned during remission phase, none showed any Eu-VSOP enhanced lesions.

We then scanned six mice as described before at day 28 p.i., corresponding to the relapse phase. The four mice that suffered clinical impairment at this timepoint showed Eu-VSOP hypointensities in T2*-weighted images. The bottom set of figure 9 illustrates an example of the same mouse that was scanned in remission phase (upper set) and again during relapse (bottom set of images). Clinical relapse symptoms in this mouse were tail paralysis and impairment of the righting reflex (EAE score 2) and corresponding MR-images showed lesions in shape of multiple focal signal extinctions throughout the forebrain, midbrain, cerebellum and CP. No Eu-VSOP accumulations could be detected in mice that were scanned without showing clinical signs of relapse at day 28.

Consistent with our previous findings on the ability of VSOP to highlight early involvement of the CP in EAE, MR-images of sick EAE mice in this study showed repeated hypointensities in the ventricles during relapse phases of disease, but not in remission. VSOP signal extinctions were found in ventricles, indicating an involvement of the plexuses, and also in meningeal zones, as shows figure 9. These pathological alterations could not be identified in Gd-contrasted images.

Eu-VSOP highlight EAE pathology corresponding to clinical symptoms. Signal hypointensities were found in the CP during relapse phases, but not in remission. Thus, our data indicate that the CP may be also involved in the re-initiation of the disease, i.e the development of relapses

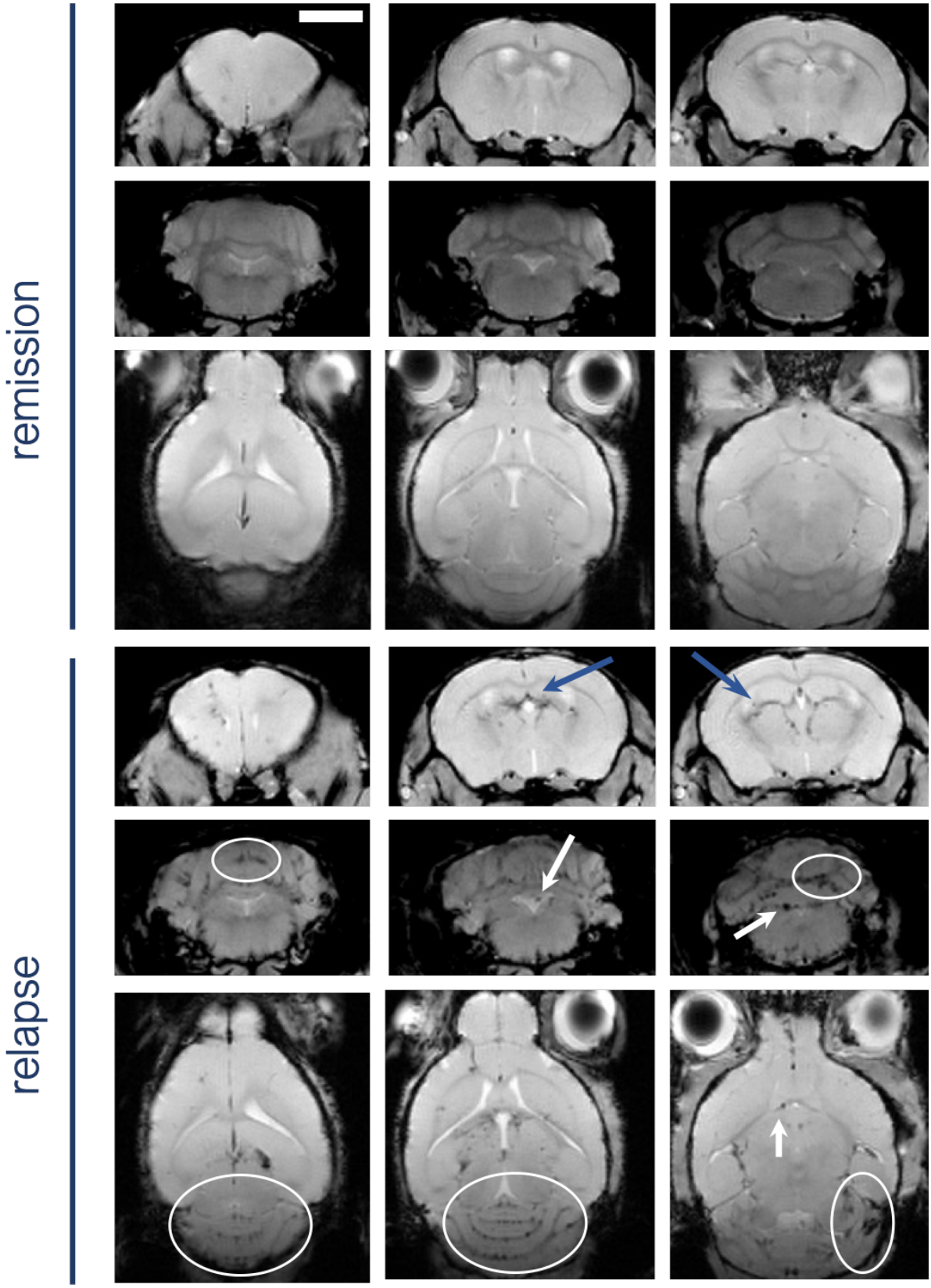

Figure 9. Monitoring of BCSFB breakdown and inflammatory pathology through detection of Eu-VSOP during remission and relapse phases in RR-EAE. T2-weighted images in coronal and sagittal orientation. MRI of a representative, previously symptomatic mouse, in remission phase (EAE score = 0) show absence of Eu-VSOP enhancing lesions (upper panels). The same mouse was scanned 7 days later, during clinical relapse phase (EAE score = 2). Scans show extensive accumulations of*

Eu-VSOP in form of focal hypointensities in midbrain, cerebellum and the ventricles with CP (bottom images). Scale bar = 2 mm. [58]

Histological evidence of inflammation and BCSFB alterations during different stages of EAE with Eu-VSOP

Our group has previously published work on the early involvement of the CP during EAE visualized by VSOP. After confirming that Eu-VSOP served to monitor BCSFB alterations and EAE lesions in vivo, in order to compare VSOP and Eu-VSOP in conventional histology, we processed tissue of this previous study and after staining for H&E (Fig. 11 A) and we applied Prussian blue and DAB intensification. An example of VSOP staining is shown in figure 10. We reaffirmed that VSOP bind to the CP in early stages of EAE when inflammation is absent and thus serve to visualize the BCSFB-breakdown prior to accumulations in other brain regions. In the present EAE experiment, we used Eu-VSOP to associate in vivo findings to histological analyzes in later stages of disease. Therefore, conventional staining for iron was performed on tissue from mice at peak disease and confirmed, that these particles are detectable through Prussian blue staining (Fig. 10 C). Then, Eu-VSOP were visualized in fluorescent microscopy, where they were detected in the inflamed CP (Fig. 10 D).

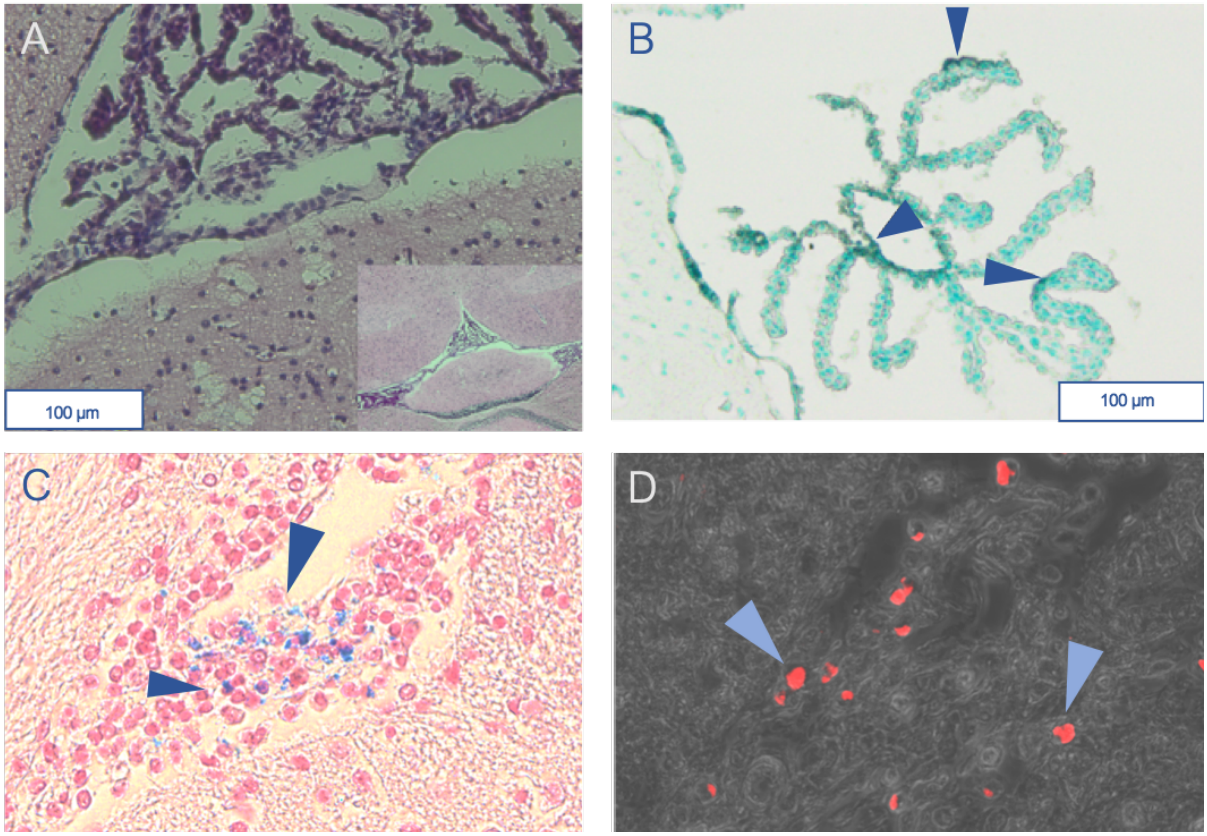

Figure 10. Histological detection of nanoparticles in EAE lesions at sites of BCSFB. A: Representative image of a healthy CP in H&E staining. B: VSOP detection by Prussian blue staining with DAB intensification highlights BCSFB CP involvement in

an EAE mouse with no clinical signs and no visible lesions (arrows).. C&D: Eu-VSOP can be visualized by Prussian blue staining for iron detection (C) and in fluorescent microscopy, here overlaid with the phase contrast image (D, serial section). At peak disease, Eu-VSOP are detected in the inflamed CP. C,D published in [58]

Eu-doped VSOP are apt to visualize histopathology when excited in a fluorescence microscope without need of a supplementary antibody. Figure 11 shows histological images of the process. Using fluorescent microscopy, we observed frequent Eu-VSOP deposition in the cerebellum of mice at peak disease, visualizing mild and more severe disseminated inflammatory lesions (Fig. 11, A-B). Fluorescent microscopy also revealed Eu-VSOP enhancing lesions in midbrain (Fig. 11 C) and meningeal inflammation (Fig. 11 D).

Our data shows that Eu-VSOP evidence inflammatory processes throughout the brain using fluorescent microscopy in peak stages of EAE.

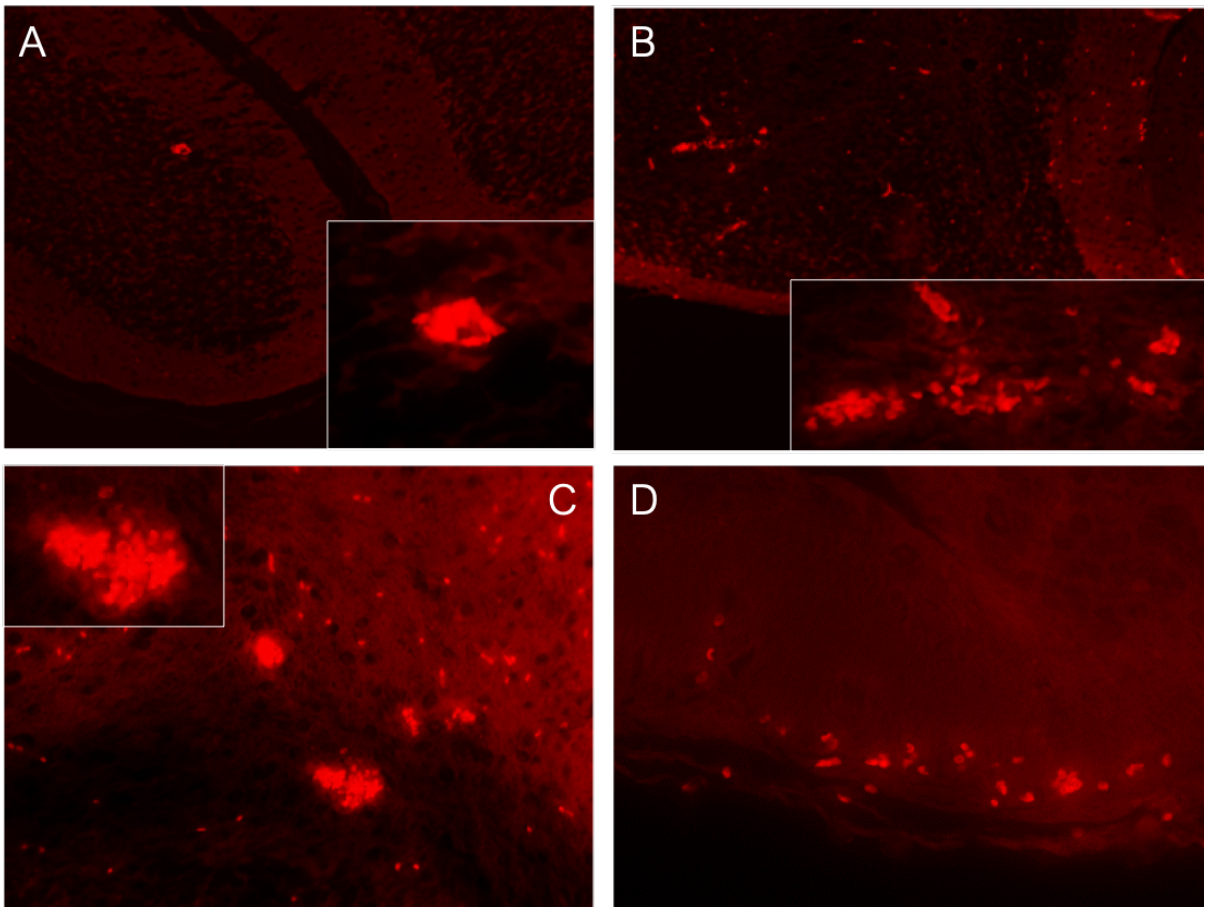

Figure 11. Detection of Eu-VSOP using fluorescent microscopy. Representative examples of Eu-VSOP accumulations in inflammatory lesions. Lesions were seen in mild (A) and more severe disseminated forms (B) in cerebellum. Pathological fluorescent signal from Eu-VSOP-labeled cells was also observed in cerebrum (C) and meninges (D) of a mouse at peak disease. [58]

Identifying histological correlates of an altered CP using Eu-VSOP

Fluorescent imaging and MRI findings in this study repeatedly indicated that Europium-doped VSOP detect the involvement of the CP in the maintenance of neuroinflammation and in relapses. Hence, we subsequently aimed to further investigate the histological correlates of an altered CP, notably the exact binding sites of Eu-VSOP in late disease stages. Therefore, we analyzed serial slides of brain tissue from mice of the same EAE experiment at peak disease under a fluorescent microscope. Confirming our observations in conventional histology, fluorescent imaging showed accumulation of Eu-VSOP in the CP of lateral (A) and fourth ventricles (Fig. 12 A, E). We then questioned ourselves about potential cells associated to Eu-VSOP in the CP. As previous studies showed that VSOP are able to be phagocytosed by macrophages, we aimed to confirm that VSOP are colocalized with these cells in the CP staining for F4/80 positive macrophages and monocytes. We also explored a potential colocalization of Eu-VSOP with CP epithelial cells using staining for pan-cytokeratin. Merging Eu-VSOP fluorescent signal and immunofluorescence, we found a fluorescent detection of pathological Eu-VSOP accumulation mostly in the CP stroma, where Eu-VSOP were often colocalized with F4/80-positive cells or in their close proximity (Fig. 12 A-H). But importantly, Eu-VSOP were occasionally linked to CP epithelial cells, that were visualized by pan-cytokeratin immunostaining (Fig. 12 I-L).

Therefore, our data suggests that Eu-VSOP not only highlight alterations of the BCSFB when phagocytosed by macrophages, but show its breakdown by visualizing the altered epithelial layer of the CP.

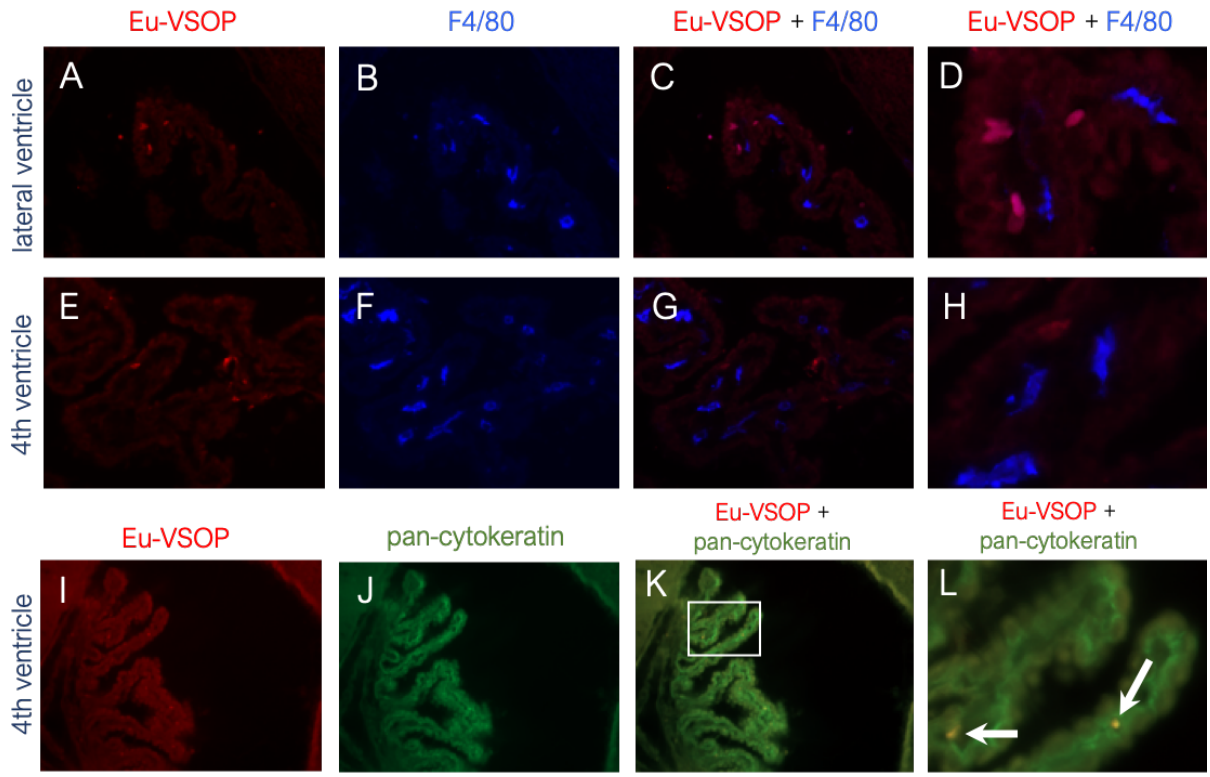

Figure 12. Combination of Eu-VSOP and immunofluorescent histology. Eu-VSOP reveals pathological cell accumulation in the CP of the lateral (A–D) and fourth (E–H) ventricles, during the relapse phase of EAE. Eu-VSOP fluorescent detection (A,E) was combined with immunofluorescent staining for F4/80 to detect macrophages (B, merge in C, D), and with pan-cytokeratin, to mark the CP epithelium (F, merge in G, H). Some F4/80-positive cells colocalized with Eu-VSOP (arrows, D). In other cases, Eu-VSOP appeared to be directly associated with the CP epithelium (H). A-H published in: [58]

II. A) Viscoelastic alterations during EAE reflect tissue remodeling at the NVU

MRE is a less invasive method of alternative imaging that our group has been working on over the past years. Even if GBCA-supported MRI does visualize one important aspect of neuroinflammation in vivo, notably BBB disruption or more specifically BBB leakage, MRE is able to distinguish further characteristics of neuroinflammation and tissue damage in a safe way. Our group has first shown the applicability of cerebral MRE in EAE and its sensitivity to early tissue alterations from inflammatory processes in the SJL model as well as its normalization during clinical recovery phases [34]. By analyzing viscoelastic alterations of the brain tissue, MRE sheds light on characteristics of EAE that contrast-enhanced MRI doesn't identify, such as tissue remodeling. In previous studies, our group has shown that a reduction of viscoelasticity in IFNγ$^{-/-}$ mice with a chronic-progressive, severe EAE, correlates with

disease activity. In addition, we showed that MRE alterations are associated to F4/80 gene expression of macrophages in the same model [44]. In this study, we questioned how RR-EAE affects viscoelasticity of the brain in SJL mice. We hypothesized, that MRE could be a useful tool to monitor neuroinflammation and that it was able to visualize further aspects of BBB disruption that GBCA-enhanced MRI does not detect. The following data was collected in collaboration with S. Wang, J.M. Millward et al. and is currently in process of publication. The study was led in two different experiments (denominated second and third block in the method section), in which the first part analyzed viscoelastic changes and histopathological alterations of the ECM in EAE and the second part further investigated these ECM alterations at different stages of EAE.

Different brain regions and EAE type shape viscoelastic properties of the mouse brain

In our previous studies, viscoelastic changes depended on the type of EAE induced: While C57/BL6 mice showed no alterations of mechanical properties of the brain during EAE, the more severely affected IFN$\gamma^{-/-}$ mice, as well as SJL mice with a relapsing-remitting course, showed extended reduction of viscoelasticity[44], [34]. Here, our objective was to confirm our previous data on reduced viscoelasticity during RR-EAE in SJL mice in a sagittal plain, which also allows the discrimination between cerebellum and other areas of the brain. Mice developed a typical relapsing-remitting disease course, with clinical signs starting around 9-10 days post immunization. Peak disease was generally reached 3-4 days later (day 12-14 p.i.) and marked the start of MRE measurements, once clinical signs were well established in all mice (Fig. 13 A). Non-immunized mice served as naïve controls. MRE was performed in one midsagittal slice of 2mm and confirmed our previous findings in coronal orientation: At day 14-15 p.i., mice showed a significant reduction of the overall viscoelasticity (|G*| magnitude modulus), as well as the elasticity (storage modulus G') and the viscosity (loss modulus G") compared to healthy controls (Fig. 13 B-D). Whereas MRE data showed an overall reduction of viscoelastic values of brain tissue, no changes in the phase angle φ were observed, indicating that the pathology had not induced severe changes in tissue architecture at this stage.

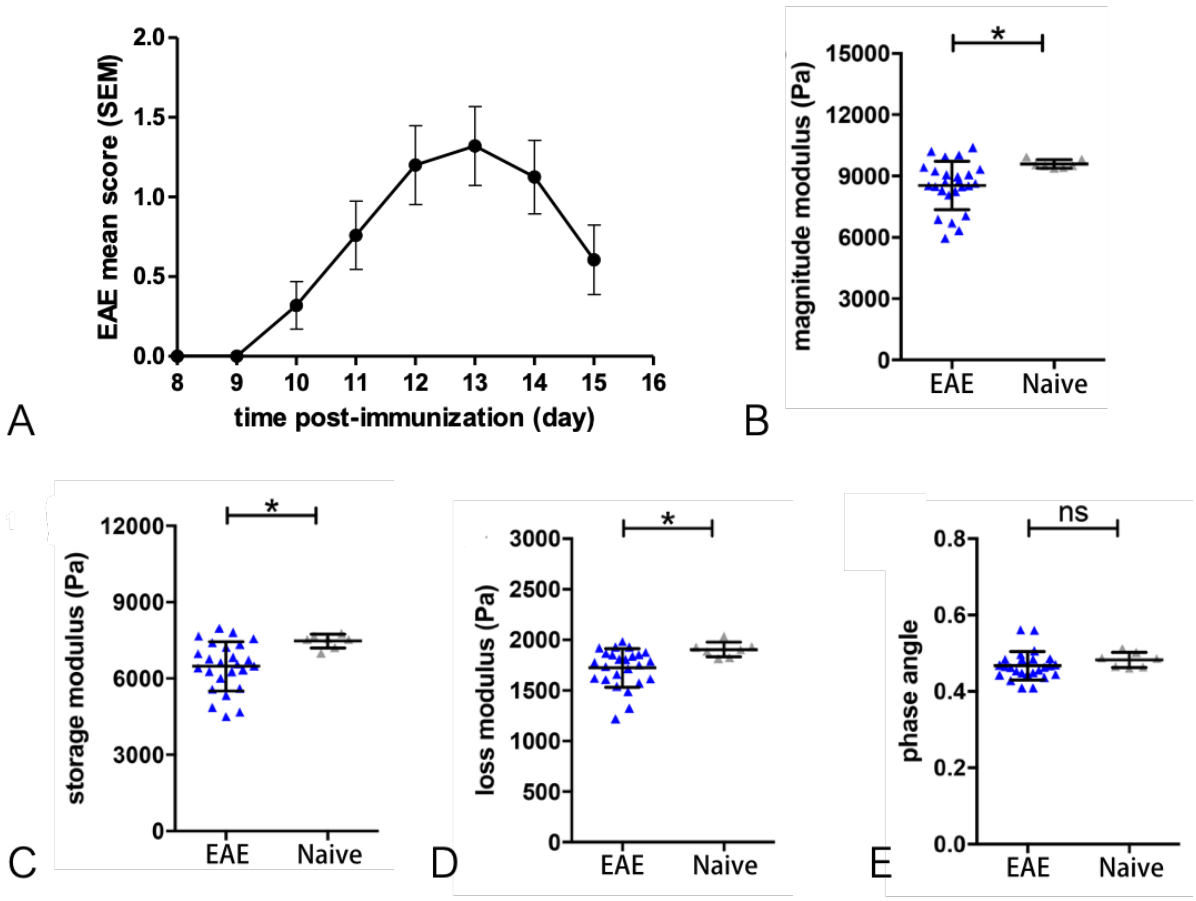

*Figure 13. Brain viscoelasticity of RR-EAE mice and healthy controls .(A) Clinical EAE score of SJL mice over time. Peak impairment was reached at day 12-14 after immunization, mean with standard error of the mean (SEM). MRE measurements at peak disease vs. healthy controls: EAE mice showed significant reductions of magnitude modulus (viscoelasticity, B), storage (elasticity, C) and loss modulus (viscosity, D), compared to naïve mice. (E) No alteration of the phase angle was observed in EAE mice. Data from five independent experiments including RR-EAE mice n=25 and healthy controls n=7 .Unpaired two-tailed t-test, *p < 0.05, mean ± standard deviation (SD).*

We previously found in the C57/BL6 EAE model that different brain regions show distinct mechanical properties: the cerebellum is significantly softer than the cerebrum [44]. Here, we hypothesized that this was accurate in SJL mice and RR-EAE as well, as the relapsing-remitting disease form is known to affect the cerebellum more severely than the cerebrum. To clarify this, on day 14 p.i. MRE data was acquired in midsagittal slices, allowing to define ROI to evaluate viscoelastic properties of the cerebrum and cerebellum individually (as shown in Fig.14 A). As expected, the cerebellum of animals during RR-EAE showed a striking reduction of viscoelastic properties, i.e. magnitude, storage and loss moduli, when compared to the cerebrum (Fig. 14 B). The values for the phase angle φ remained stable in both regions.

In this RR-EAE study, we also calculated the viscoelastic changes in SJL mice in separate regions in relation to sex and age matched healthy controls to assess the impact of inflammatory disease on each region. Figure 14 C shows: both investigated regions, cerebellum and cerebrum

undergo reductions in viscoelasticity during RR-EAE normalized to healthy controls, as indicated by mean difference $\Delta|G^*| < 0$. However, although the brain as a whole gets "softer", the magnitude modulus diminished most notably in the posterior region, suggesting a more pronounced loss of brain stiffness in the cerebellum, that is known to be more susceptible to inflammatory pathology than the rest of the brain in the present EAE model.

During RR-EAE, the brain experiences a reduction of viscoelastic values. MRE recognizes changes of viscoelasticity especially well in the cerebellum, which is more severely affected by inflammatory processes in this model.

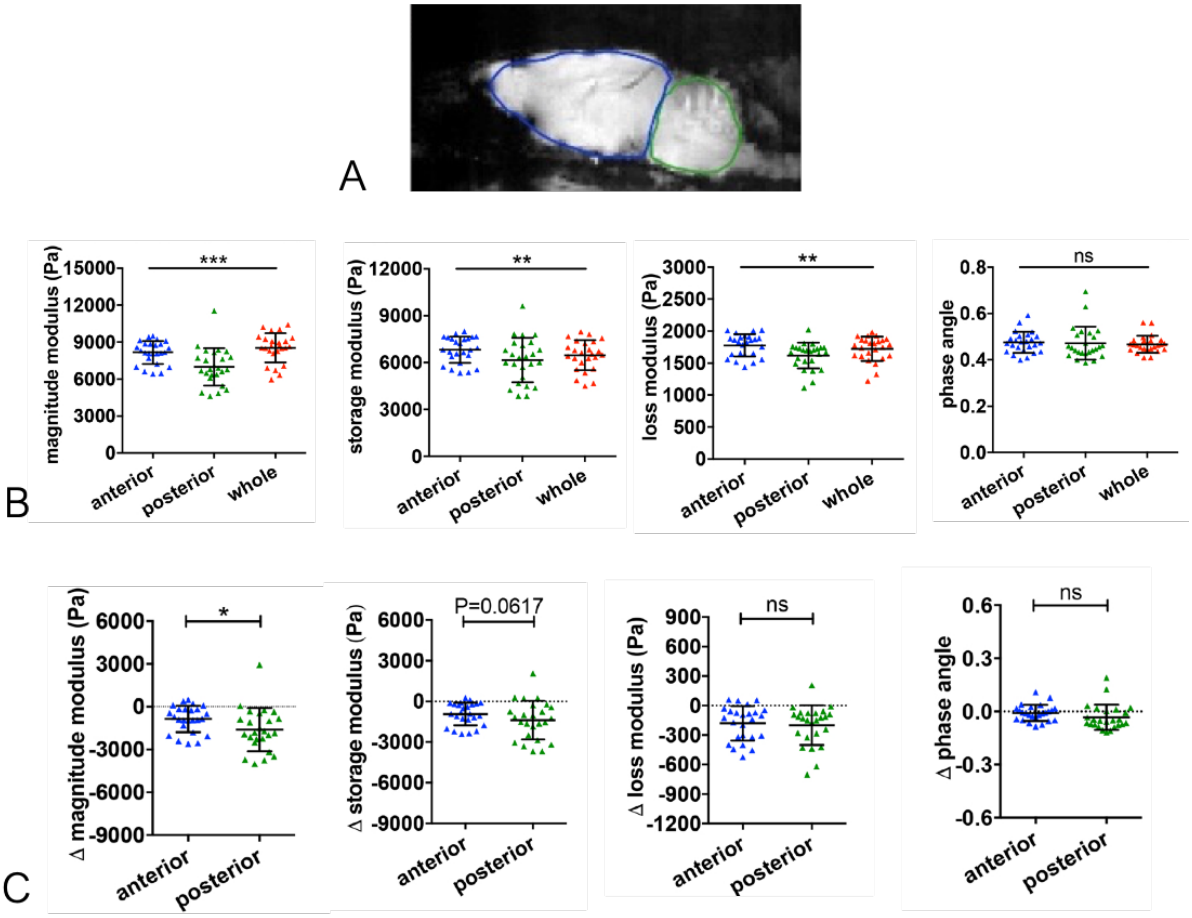

*Figure 14. Comparisons of viscoelasticity in distinct brain regions. (A) A representative midsagittal slide of an EAE mouse shows a magnitude image with definition of ROI: blue = anterior and green = posterior (B) Comparison of the viscoelastic properties of the posterior/cerebellar region with the anterior region and the whole brain during inflammation. Repeated measures ANOVA, *** $p < 0.001$. (C) Δ MRE values of anterior and posterior brain regions at peak EAE normalized to the values of age- and gender-matched healthy controls. The magnitude modulus is particularly diminished in the posterior region (cerebellum) compared to the anterior region (cerebrum). Data from five independent experiments n=25. Paired two-tailed t-test, * $p < 0.05$, mean ± SD.*

Severity of clinical impairment influences viscoelastic properties

As mentioned in the introduction, prior research as well as clinical experience has repeatedly outlined the frequent discrepancy between clinical disability and MRI measurements, in MS [57] as well as EAE [17]. In this work, we evaluated if MRE alterations correspond with the severity of EAE symptoms and observed that a reduction of viscoelasticity shows a significant correlation with the clinical EAE score. Correlations between magnitude and storage moduli and the clinical score of EAE mice at the time of MRE measurements showed values of p=0.0117, r=-0.6306 and p=0.0373, r=-0.5411, respectively (Fig. 15 A, B). We did not find significant correlations between loss modulus or phase angle φ on one side and clinical EAE scores on the other.

MRE measurements correlate with EAE clinical scores and are therefore apt to monitor disease course in RR-EAE.

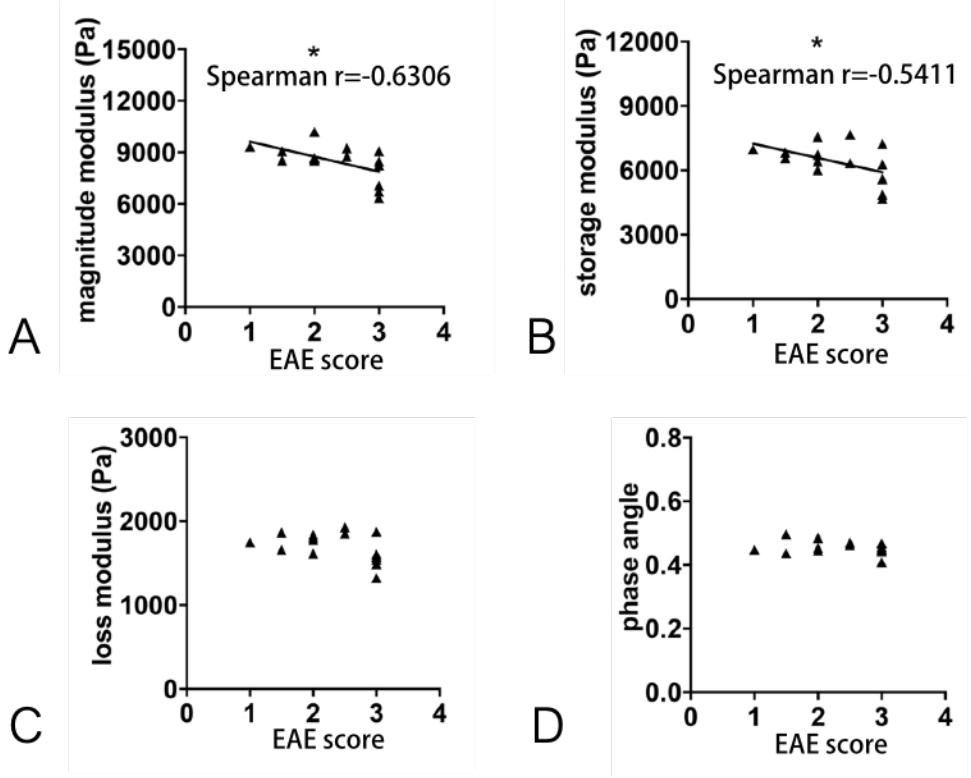

*Figure 15. Correlation of EAE clinical score and viscoelastic properties of the brain. (A) Negative correlation between clinical EAE score and magnitude modulus (p=0.0117, r=-0.6306) as well as (B) storage modulus (p=0.0373, r=-0.5411). No correlation with (C) loss modulus and (D) phase angle. Data from five independent experiments, including only symptomatic mice, n=15. Spearman correlation, * p < 0.05.*

MRE does not correlate with gadolinium enhancement in acute EAE lesions

To date, GBCA-MRI represents the standard approach to identify BBB breakdown in MS patients and also in animal models. In order to compare the ability of MR-based imaging for its

ability to detect inflammatory lesions, we investigated in the same RR-EAE mice, whether the intensity of Gd enhancement in MRI correlates with clinical scores and viscoelastic values in MRE. 24 hours after MRE measurements, coronal and axial oriented T1-weighted images were acquired before and after injection of 0.2mmol/kg Gd contrast agent. Acute pathology in active EAE is seen as diffuse hyperintensities distributed through the brain, which can complicate the identification of lesions. To better recognize the extension of these disseminated lesions, our group generated T1 maps allowing to make a quantitative analyze of contrast changes resulting from GBCA leakage. Representative images illustrating the T1 maps before and after GBCA administration are shown in figure 16 A. As expected, due to hyperintense lesions, the post-contrast T1 values for all mice were significantly reduced compared to the pre-contrast values. But surprisingly, there was no significant correlation between Δ T1 (difference between mean pre-contrast and mean post-contrast) and the magnitude modulus (p=0.8797, r=0.05181, Fig. 16 B) or between signal intensity changes and viscoelasticity (p=0.3402, r=0.2315, Fig. 16 C). We did not find a significant correlation between T1 signal intensity changes and EAE clinical scores, consequently (p=0.2325, r=-0.4195, Fig.16 D).

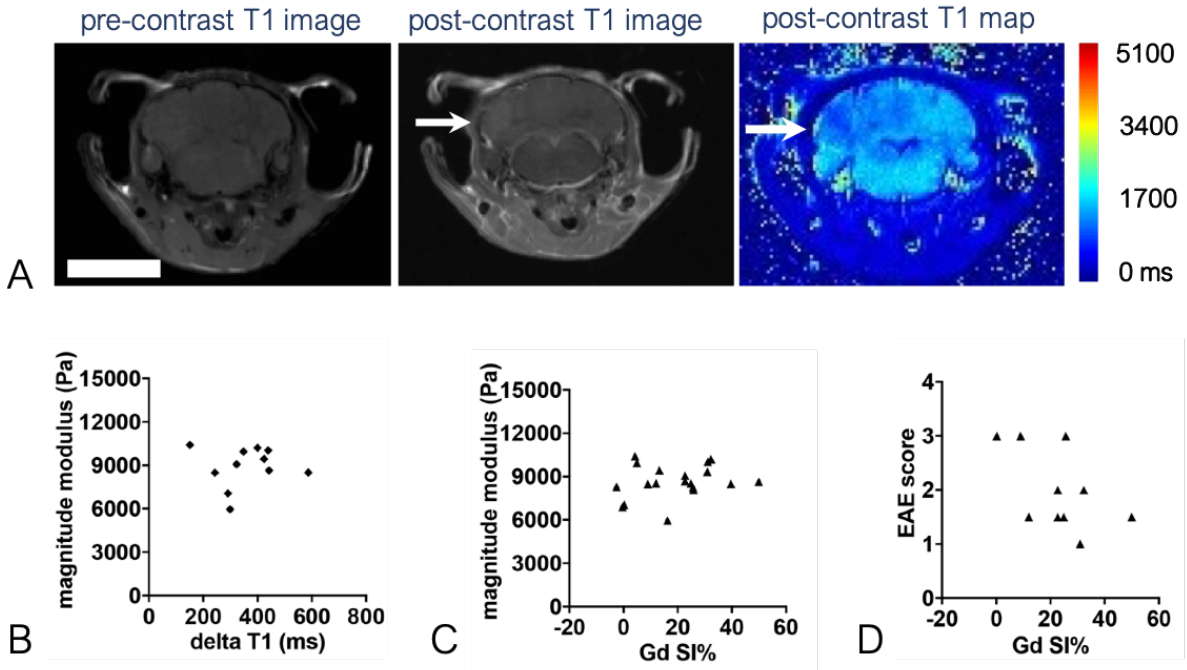

Figure 16. Comparison of whole brain contrast-enhancing lesion burden with whole brain viscoelasticity. Representative coronal T1-weighted MR images before (left) and after (middle) GBCA administration. A diffuse hyperintense lesion is seen in the cerebellum (arrow). T1 map (right) post-contrast with T1 relaxation time in ms. Scale bar = 5 mm. (B) No correlation is seen between Δ T1 (mean pre-contrast minus mean post-contrast) and the magnitude modulus (Pearson correlation, p=0.8797, r=0.05181). (C) T1 signal intensity changes (SI%) obtained from the T1-weighted images following Gd application showed no correlation with the magnitude modulus (Pearson correlation, p=0.3402, r=0.2315). (D) There was no significant correlation between SI% and the EAE score (Spearman correlation, p=0.2325, r=-0.4195). Data from two independent experiments, n=11 and n=19 in (B) and (C), (D), respectively.

Viscoelastic changes are associated to altered gene expression of the ECM molecule fibronectin

As mentioned in the introduction, one important compartment shaping the viscoelastic properties of the brain during neuroinflammation is the extracellular matrix. In this study, we aimed to explore whether viscoelastic changes may reflect processes of tissue remodeling at lesion sites and if specific alterations of the ECM could be linked to MRE changes. Performing qPCR analyzes in brain tissue of the same EAE mice, we found a significant correlation between a reduction in brain stiffness and an increased expression of the ECM proteoglycan fibronectin (Fn), p=0.0041, r=-0.9473 (Fig. 17). This correlation was confirmed in frozen tissue of an EAE experiment, in which we collected MRE data in coronal sequences [34], p=0.0163, r=-0.6737.

We considered if the association of MRE changes and Fn expression could be extended to other ECM components and investigated the gene expression of other key proteoglycans of the brain ECM involved in decisive neuropathological events associated to BBB alterations during neuroinflammation (e.g. Glypican 5) and remodeling of the perineuronal and parenchymal matrix (e.g. neurocan and brevican). We found no correlation between viscoelastic measurements and the expression of these ECM molecules, p=0.9755 and r=-0.01632, p=0.3062 and r=-0.5056, p=0.8671 and r=-0.08886, respectively (Fig. 17 C). We then asked ourselves how the correlation between MRE and Fn expression behaves during different phases of the relapsing-remitting disease. Therefore, we performed qPCR analysis in the frozen tissue from our previous EAE study in SJL mice in which we acquired MRE data in coronal sequences at two timepoints: peak disease and remission phase [34]. Interestingly, we found a significant correlation between the Fn expression at peak disease (day 14) and the phase angle φ (Fig. 16 D), that disappeared in remission (day 28), indicating alterations in tissue architecture correlating with the Fn expression, that may regress in remission phase. In this previous study, we observed that MRE tissue alterations correlated with the amount of infiltrating T cells. [34]. Here, we explored if the Fn expression could be associated to higher amounts of inflammation. We found a significant correlation between Fn expression and expression of $CD3e^+$ T cells, indicating high amounts of Fn being associated to greater T cell infiltration (Fig. 17 E).

Thus, our data indicates that “softening" of the brain is associated to an increased expression of Fn. Changes in the architecture of tissue as shown by phase angle φ are associated to an increased Fn expression during peak disease, but not in remission. Fn expression is enhanced when more inflammation with infiltrating T cells occurs.

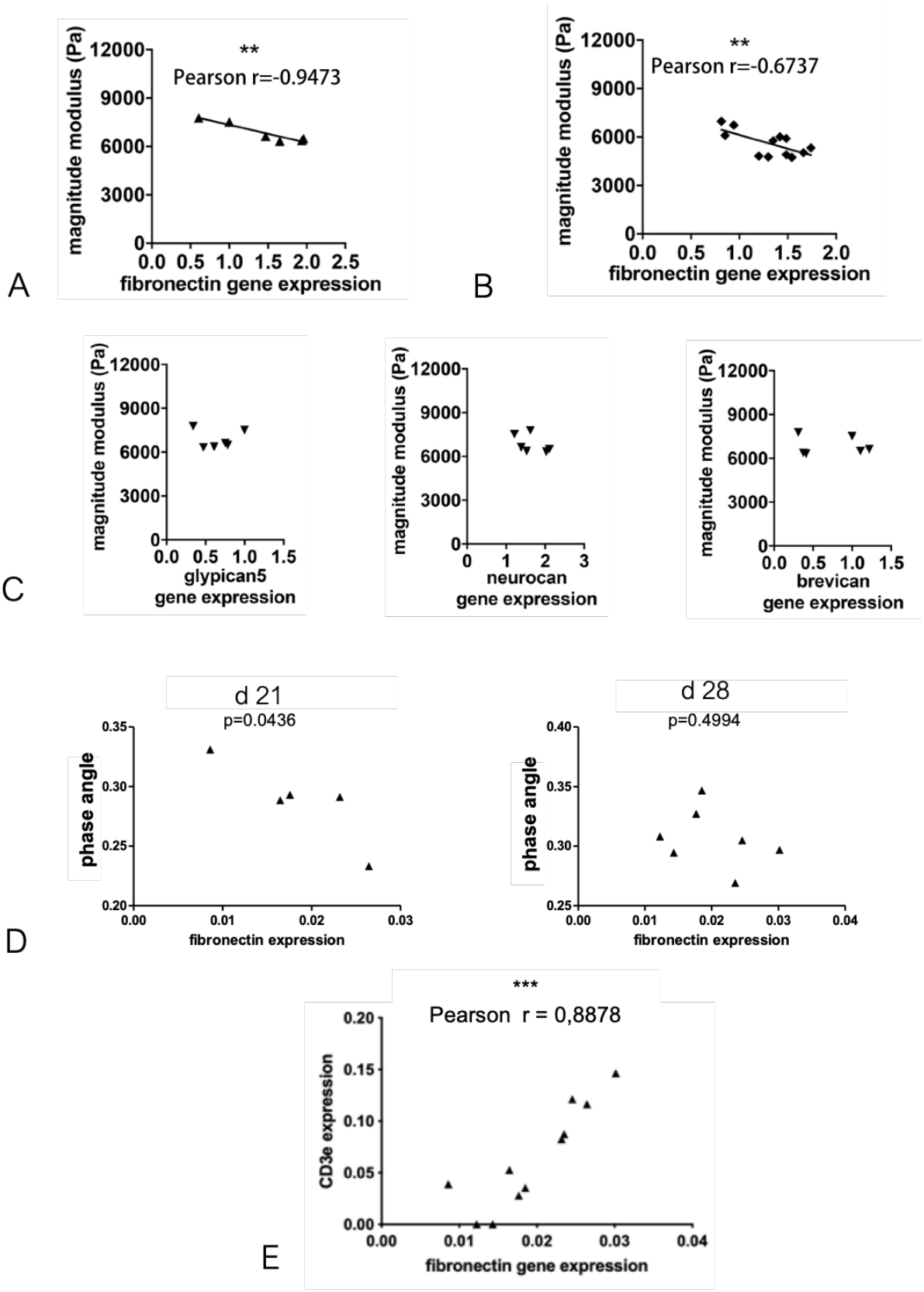

Figure 17. Association between viscoelastic changes and expression of FN. (A) The degree of reduction of cerebellar rigidity (magnitude modulus) at EAE peak is associated with increased expression of Fn assessed by qPCR, p=0.0041, r=-0.9473. (B) The same association between magnitude modulus and Fn expression was found using frozen tissue from our previous in SJL

*EAE with coronal MRE. p=0.01163, r=-0.6737. (C) No correlation was observed between cerebellar magnitude modulus and gene expression of other ECM components of the cerebellum including glypican5, neurocan and brevican respectively. Pearson correlation, * p < 0.05, ** p < 0.01. Data from two independent experiments, including only symptomatic mice, n=12 and n=6 in (B) and (A), (C), respectively. D: Fn expression correlates significantly with the phase angle at day 21, peak disease, but this correlation is not found at day 28, remission phase. E: Correlation between Fn gene expression and CD3e. During RR-EAE. Fn expression correlates with CD3e expression for T cells. p= 0.0003, r = 0,8878.*

Remodeling of the NVU as evidence of BBB disruption

To validate our hypothesis that increased Fn gene expression is due to increased protein deposits in brain lesions, the corresponding tissues to MRE experiments were processed for Fn immunofluorescence staining. In these brain tissues of mice at peak disease of RR-EAE, we found pronounced Fn deposits in perivascular cuffs. The Fn proteoglycan comes in two forms, containing alternatively spliced domains: plasma fibronectin (pFn) leaks out of the vessels following BBB disruption. Cellular fibronectin (cFn) contains the alternatively spliced domains EIIIA and EIIIB, in the brain it is primarily synthesized and released by astrocytes[63]. In this study, we hypothesized that Fn deposits in EAE lesions may arise from local cells rather than from circulating pFn. Thus, to explore the source of the proteoglycan accumulations, we used an EIIIA-Fn antibody to detect cellular Fn and combined it with the broad-spectrum anti-Fn antibody. The staining result showed a consistently overlapping pattern, indicating that Fn deposits have indeed a cellular origin and are produced in perivascular areas (Fig. 18 A). To clarify how astrocytes and Fn deposits may be colocalized, we costained with the astrocyte marker GFAP. The combination showed interestingly, that not only astrocytes but also endothelial cells of the BBB may be a major source of cFn associated to EAE perivascular lesions (Fig. 18 B).

As Fn is predominantly found in perivascular lesions at peak EAE, from cellular origin and partly associated to astrocytes surrounding microvessels, this data indicates a process of remodeling around the NVU that involves astrocytes as well as endothelial cells of the BBB.

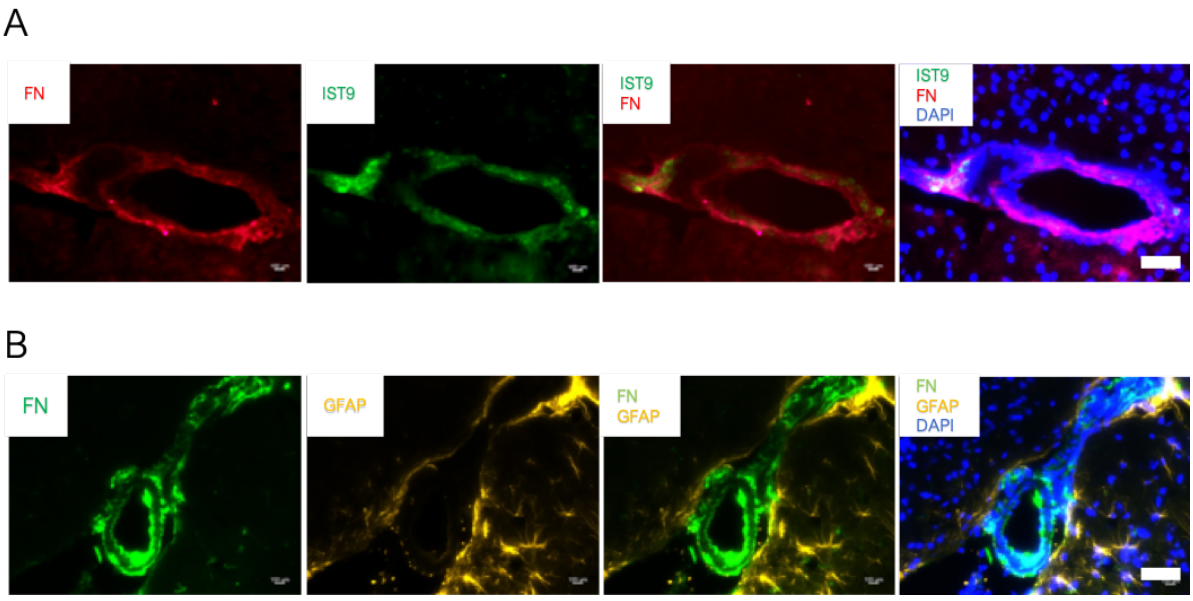

Figure 18. Histological colocalization of Fn. (A) Immunostaining with anti-Fn for detection of overall Fn (red), and anti-EIIIA-Fn for detection of cellular Fn (IST9, green) indicates that perivascular Fn deposits are secreted by cells. Cell nuclei are blue. Scale bar=100µm. (B) Immunostaining of Fn (green) and the astrocytic marker GFAP (yellow) shows perivascular astrocytes adjacent to the Fn deposits in the EAE brain. Cell nuclei are blue. Scale bar=100µm.

II. B) Visualizing perivascular Fn aggregates through disease course

We thereupon wanted to investigate in brain tissue how the Fn aggregates evolve in remission, as the correlation that we had found between Fn expression and the phase angle φ of mice at peak disease regressed in remission phase, indicating Fn deposits may change through disease course. We performed immunostaining in tissues of SJL mice at peak phase and remission of EAE, after staining for H&E as an overview method to identify lesions and ROIs. SJL mice showed EAE lesions predominantly in the midbrain and cerebellum. In immunostainings, we stained for Fn and used DAPI as a counterstain to identify EAE lesions (Fig. 19 upper set of images). As a result, we found Fn deposits in both phases of disease, including remission. In all stages of disease, Fn deposits were predominantly found in EAE lesions. No Fn deposits were found in the brain parenchyma in control tissue. A thin layer of Fn was visible in bigger vessels.

In peak disease, Fn was found in all perivascular lesions, although pathology affected predominantly posterior regions of the brain. Fn deposits were especially pronounced in perivascular cuffs and in smaller amounts throughout the parenchyma. More pronounced Fn deposits were associated to infiltrating cells around the perivascular space, i.e. to a more severe inflammation (Fig. 19, D-F). During remission, Fn deposits were visible at perivascular sites

and associated to regressing lesions. But interestingly, Fn deposits in close vascular proximity were thinner and instead spread more diffusely into the parenchyma. Fn deposits associated to lesions reached extensively into the granule cell layer of the cerebellum (Fig. 19, G, H). Notably, Fn was also found in the NAWM distant to perivascular lesions and visible infiltrating cells, indicating Fn may be redistributed during remission (Fig. 19, I).

Fn deposits at peak disease are predominantly found in perivascular cuffs, but in remission they spread more diffusely into the brain parenchyma and the NAWM. These findings indicate that Fn deposits are being disassembled and redistributed in phases of low inflammatory activity.

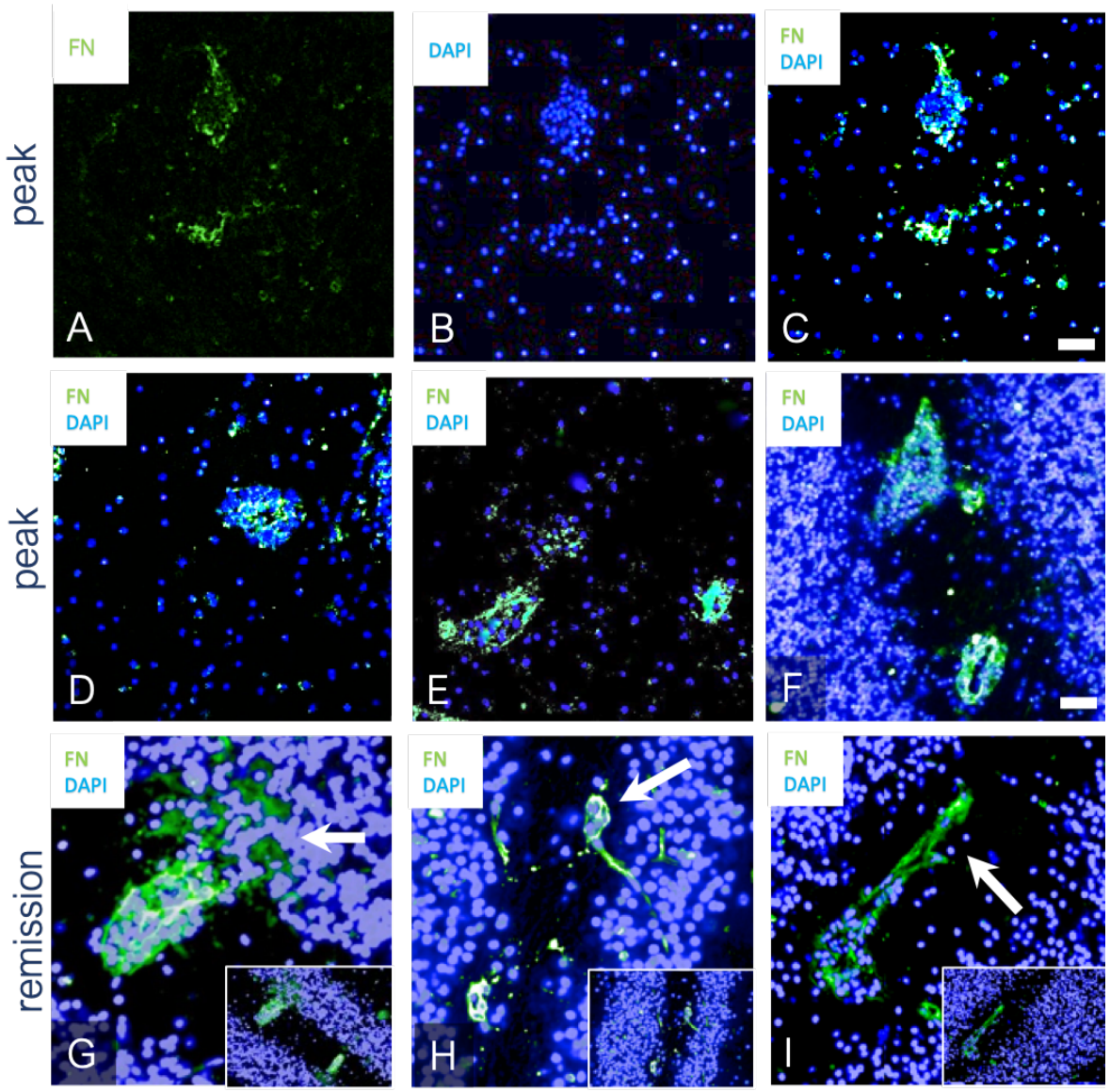

Figure 19. Fn deposits during EAE course. Immunofluorescence staining at peak disease, costaining of Fn in green and cell nuclei in blue to identify EAE lesions (upper set of images). EAE lesions during peak disease are found in midbrain(D,E) and cerebellum (F) and primarily confined to perivascular areas. During remission, Fn deposits are predominantly found in the

cerebellum (bottom set). Accumulations spread diffusely into granule cell layer (G) and deposits in direct vascular proximity were limited to a thin band (H). Protein deposits reached beyond lesions into NAWM (I). Scale bar=100µm.

Discussion

In recent years, data has been accumulating that brain barrier breakdown is a decisive step in the initiation and maintenance of neuroinflammation. Conventional imaging methods in MS and EAE, like GBCA-enhanced MRI, have limitations that where thoroughly assessed in the introduction. The primary objective of this study was to monitor brain barrier alterations in the relapsing-remitting model of EAE by novel MR techniques in vivo and to correlate them to histopathological findings.

Eu-VSOP highlight alterations of the BCFSB

The development of innovative contrast agents with multifunctional properties has critically influenced the research on visualization techniques of neuroinflammatory diseases in recent years. With regard to the challenges of clinical imaging and in order to understand the variety of presentations of CNS alterations, the necessity of developing methods linking in vivo findings to histopathological processes has become a central ambition. It has propelled to the forefront experimental multimodal contrast agents that are simultaneously detectable in T1 and T2 weighted MRI and by optical imaging methods.

One of these methods, that we used in the present study, are Europium doped VSOP. In order to visualize disruption of brain barriers, we applied the nanoparticles to EAE mice in different stages of disease. Given their property to detect neuroinflammatory pathology in MRI in vivo and connect them post mortem to various histological analyzes, nanoparticles were an excellent imaging method for our purpose. Our group and others showed previously in the EAE model that electrostatically stabilized VSOP are apt for in vivo detection of different pathological and immunological characteristics of CNS inflammation, notably phagocyte activation and recruitment, alterations of the brain extracellular matrix and activation of brain endothelial cells [23, 27-29]. It was further demonstrated that the use of Eu3+ combined VSOP allows a multimodal use of the nanoparticles: the nanoparticles serve as a negative contrast agent in MRI while, on account of their Europium core, acting as a luminophore with excellent results in fluorescent microscopy and further enabling a quantification through spectrophotometry [60, 64-66]. Hence, this study benefits of the double potential of Eu-VSOP: to visualize the characteristics, distribution and development of neuropathological events – notably alterations of the BCSFB – in vivo by MRI, and to analyze these processes with histopathological methods ex vivo.

The customized HEE antenna solution developed by the radiology department of the Charité allows the detection of Eu-VSOP in conventional fluorescence microscopy, as well as their combination with antibodies for immunofluorescent staining. Conveniently, false positive stainings due to unspecific binding as they are known from antibody-based methods do not occur. Nevertheless, it should be noted that the excitation wavelength of Europium – 350 nm – overlaps with the ones of nuclear stainings such as DAPI (358 nm) or Hoechst (361 nm) and thus excludes the combination with these conventional DNA dyes. However, alternative nuclear stainings such as Topro-3 might be suitable for future studies using Eu-VSOP.

Concerning the uptake of our nanoparticles, Kobayashi et al. showed that Eu-VSOP were as efficiently taken up by RAW264.7 macrophages as their precursor without an Eu3+ core [66]. Our group showed previously that brain endothelial cells are able to endocytose VSOP under inflammatory stimuli [29] and affirmed in the present work, that this is valid for Eu-VSOP too. The particles were spontaneously taken up by bEnd.3 cells in culture and this effect was increased under stimulation with TNFα [58].

In this work, we demonstrated that Europium doped nanoparticles are able to visualize EAE lesions in vivo and that their capacity to identify pathology is comparable to the one of non-Europium VSOP used in previous studies [27]. Importantly, we demonstrated that Eu-VSOP are suitable to monitor disease activity in the relapsing-remitting model of EAE by visualizing CNS alterations. Through peak, remission and relapse phases of disease, MR-hypointensities by Eu-VSOP correlated with the clinical impairment of animals, with no accumulations detectable during remission phase and multiple focal signal extinctions when symptoms worsened, and only then. Research using nanoparticles has increased in the last years, with the result of ongoing development of their properties. Other groups using T2-weighted MRI of USPIO, with different characteristics than our Eu-VSOP, have shown excellent results to monitor CNS alterations during first peak of EAE [67-70], but prior research also presents discrepancies between reports, such as in Rausch et al. and Berger et al., who claimed that USPIO-based MRI was not fit to monitor disease course in rats [67, 69]. Other studies could not correlate the appearance of USPIO-enhancing lesions with clinical relapses in mice [70]. Explanatory approaches for paradoxical observations may lie in the use of distinct EAE models with particularities in pathophysiology, especially between rats and mice, but also among animal strains, resulting in a variety of pathological observations. Comparison of studies is further hampered by the diversity of formulations and doses of nanoparticles along with particular detection protocols, MRI systems and differences in scanning details. USPIO present other properties than our nanoparticles, as they are importantly bigger and do not have an

electrostabilizing citrate coating. VSOP and Eu-VSOP however could be suitable to monitor EAE relapses, as they show pathological steps of EAE, such as phagocytosis, endothelial activation and CP inflammation [28, 29, 66]. Indeed, it might even be a more sensitive method for RR-EAE imaging, as the conventional GBCA contrast enhanced MRI shows typically a non-focal, diffuse enhancement in active EAE of SJL mice, while we found not only a correlation with clinical score during remission and relapse, but also a much more accurate appearance of focal hypointensities. However, the interest of Eu-VSOP lies rather in the possibilities of targeting pathological tissue changes than in their eventual clinical use, as they do visualize important pathophysiological processes, but their long-time effect in humans is yet unclear.

To further analyze pathological alterations after confirming that Eu-VSOP highlight lesions in vivo, we showed that signal extinctions correlated with histological detection of nanoparticles by conventional and fluorescent microscopy. Inflammatory lesions were identified in cerebrum, cerebellum as well as in meningeal spaces and the CP.

Recent data on neuroinflammation has increasingly shed light on specific immune processes such as CNS immune surveillance and pointed out the unique role of the CP as a neuro-immunological interface [71]. Our group showed in previous work on EAE mice, that VSOP highlight the involvement of the CP in the initiation of neuroinflammation [28]. In this study, by application of Eu-VSOP to EAE mice, alterations of the BCSFB and especially the role of the CP materialized in double form: by MRI and in fluorescent microscopy. In contrary to gadolinium, Eu-VSOP visualized the involvement of the CP in MR images during peak disease and relapse of symptoms, i.e. reinitiation of neuroinflammation. Interestingly, no hypointensities were found in the ventricles when clinical impairment diminished, indicating that the BCSFB restores itself during remission phase. Ventricle-associated hypointensities in MRI could be linked to post mortem histological analyzes of the CP using fluorescent microscopy. Combination of fluorescent detection of Eu-VSOP and immunofluorescence stainings for F4/80 determined a frequent colocalization of Eu-VSOP with macrophages/monocytes. This is not surprising, as the greater part of Eu-VSOP associated signals may result from nanoparticles inside of phagocytes or antigen-presenting cells such as CP resident dendritic cells that endocytose particles crossing the fenestrated endothelium. But interestingly, immunofluorescence of cytokeratin evidenced certain accumulations of Eu-VSOP distinct from phagocytes and instead in colocalization with CP epithelial cells, suggesting the ability of Eu-VSOP to bind directly to the epithelial layer and indicating epithelial cell alterations.

Processes concerning BCSFB disruption are not as broadly elucidated as for BBB breakdown. Correlation of leukocyte numbers in CSF of MS patients and lesion burden in MRI suggests that CP inflammation contributes to the disease, although in a partly elusive manner [72]. In the healthy CP, fenestrated blood vessels are surrounded by CP epithelial cells establishing the BCFSB. Leukocytes can pass the fenestrated endothelium but remain trapped in the CP parenchyma and rarely enter the CSF, as they would have to break through the tight barrier of epithelial cells. But during neuroinflammation, the characteristics of the BCSFB are altered and the chemokine production of infiltrated T-cells in the CP parenchyma facilitates the entry of immune cells through the epithelial layer into the CSF [73], from where they disseminate to the meningeal and perivascular spaces. Here a massive production of inflammatory mediators like proinflammatory cytokines induces an activation of endothelial cells of the brain microvasculature, resulting in a "second wave" of leukocyte recruitment through the BBB and lesion formation [71]. Thus, integrity of the epithelial barrier of the CP may be considered as a decisive factor of leukocyte-CNS entry. However, evidence on the role of CP epithelial cells in immune cell trafficking through the BCSFB is scarce. It has been known for some time that the expression of adhesion molecules such as ICAM-1 and VCAM-1 on the luminal surface of the CP epithelial cells is upregulated after inflammatory stimuli in vivo and during EAE [74]. Among other processes, expression of the chemokine CCL20, a ligand for the chemokine receptor CCR6, on CP epithelial cells was recently shown to direct CCR6+ Th17 cells across the BCSFB during the initiation of EAE [17]. As Zhang et al published in 2013, the epithelial cells of the CP express the proteoglycan syndecan-1, which is associated with CCL20 expression in EAE mice and knock-out of this heparan-sulfate proteoglycan results in higher numbers of infiltrating Th17 cells and increasing levels of IL-6 [75]. Other reports highlight the specific role of tight junction proteins like zonula occludens and claudins accompanying epithelial barrier disruption, demonstrating drastic distortion of the barrier with marker ZO-1 and a slight decrease of barrier proteins for CLN-2 in EAE [76]. In MS and EAE, the TJ protein CLDN-3 was shown to be a determinant of BCSFB integrity and its loss correlated with exacerbation of clinical symptoms [77].

The mechanisms of ingestion of VSOP and Eu-VSOP into cells are not completely elucidated either. Concerning the CP, vesicular transport through epithelial cells might be the way, as the CP epithelium shows a highly active vesicular transport, which indicates the relevance of transcytosis as a route for VSOP across the BCSFB [78]. Further potential binding sites for the nonspecific, particle-based imaging probes include not only phagocytosing cells, but also molecular components of the ECM in the form of glycosaminoglycans and the

glycocalyx, which are substantially enhanced in inflammatory tissue and altered in comparison to the healthy brain. In our previous work, we showed that VSOP binding to the endothelium is partly mediated by interactions with glycosaminoglycans on the surface of bEnd.3 cells of the BBB [29] and we hypothesize that similar mechanisms may operate in the CP.

In conclusion, current wisdom points out the crucial importance of a proper function of the BCSFB in the maintenance of CNS health and in immunosuppression. Our data is a step towards understanding pathological alterations occurring at barriers and further investigations on nanoparticles in general and specifically on Eu-VSOP binding might elucidate the processes involved in BCSFB breakdown during neuroinflammatory diseases. If the multifactorial analyze of CP with novel visualization techniques is implemented, it will allow to further enlighten the phenomena related to alterations of this important immunological interface, eventually helping to understand fundamental pathophysiological alterations occurring in various CNS disorders, even before breakdown of BBB and establishment of neuroinflammation occur.

Assessing BBB-remodeling at the NVU with MRE and immunofluorescence

The second part of this work was dedicated to the assessment of remodeling aspects in BBB breakdown through MRE. We explored the capacity of MRE to detect acute perivascular inflammatory pathology in the mouse brain during RR-EAE. Therefore, MRE measurements and T1-weighted MRI using GBCA were performed and related to EAE clinical scores. Moreover, in order to further comprehend viscoelastic alterations, we investigated molecular and histological correlations of tissue remodeling in perivascular lesions with qPCR and immunofluorescence.

Our group has previously performed viscoelastic measurements on SJL EAE and consistent with the findings in these studies using coronal MRE slices [34], we here revealed a reduction in overall viscoelasticity at peak disease compared to the corresponding healthy controls in a sagittal plane. In analogy to our findings in C57/BL6 mice [44], we demonstrated that in the SJL strain the cerebellum is softer than the cerebrum, and that these properties are maintained during EAE. The lower viscoelasticity in the mouse cerebellum is in agreement with results from other MRE investigations proving that the human cerebellum has a lower viscoelasticity than the cerebrum [79], and the further reduction during EAE is not surprising considering that the SJL model is known for affecting most severely the cerebellum, which is more susceptible for BBB disruption and lesion formation [80]. So, if RR-EAE predominantly

affects posterior regions, where in our measurements viscoelasticity was strikingly reduced, MRE is likely to especially well identify areas of severe inflammatory activity. The phase angle φ did not differ significantly between anterior and posterior part of the brain, suggesting that the complexities of the tissue architecture in the two regions are comparable and, consistent with our previous findings [34, 44], no changes in the phase angle φ were observed at peak disease, indicating that even if the tissue during EAE is prone to pathological changes in mechanical properties, the complexity of the tissue architecture remains intact, at least at the timepoint that we investigated here. Possibly, persistent tissue damage linked to chronic inflammation may cause alterations of the tissue network organization at later stages of the condition, e.g. in relapse phases. This may be a question for further studies.

Whereas in our previous study with C57/BL6 mice we could not associate clinical disability to MRE, we here found a significant correlation between brain viscoelasticity in SJL mice and EAE clinical score and confirmed the sensitivity of the sagittal MRE scans to assess neuroinflammation. While both strains show spinal cord pathology, brain and especially cerebellar involvement is more common in the SJL than in the C57Bl/6 model [80], which is reflected in MRE measurements.

Despite its limitations, notably only visualizing one aspect of BBB breakdown, which is barrier leakiness, gadolinium-enhanced MRI is still the prevailing imaging method to detect acute inflammatory CNS pathology. However, recent investigations have queried contrast-enhanced MRI, particularly because of reports pointing out potential toxic side effects of GBCA, rising the urge to find alternative imaging methods with increased sensitivity while improving understanding on pathological processes during the disease. In the active EAE model, hyperintensities caused by Gd-enhancing lesions are difficult to quantify using T1 weighted images, due to their numerous, but rather small appearance and diffuse distribution. Therefore, we used T1 mapping of images of the entire brain to allow a quantitative readout of lesion burden. GBCA shorten the T1 relaxation time and this relaxation time is directly proportional to the concentration of contrast agent in the tissue. For the T1 mapping, absolute T1 values of the brain before and after i.v. injection of Gd allow the calculation of contrast agent concentration per voxel. Other groups recently applied this strategy in a mouse brain tumor model, improving its detection by MRI [81]. Using the difference of T1 values averaged over the entire brain to measure BBB disruption also avoids potential sampling bias that might occur in the attempt to subjectively quantify lesions in selected brain slices, given the uneven distribution of brain lesions in active EAE. Surprisingly, we did not find a significant correlation between the lesion burden in GBCA-enhanced MRI and MRE measurements. This

was contrary to our expectations and emphasizes the complexity and ambiguity of pathological processes occurring at one time during EAE and underlines the necessity for further studies in order to connect information about these processes.

To enter the brain parenchyma during lesion formation, immune cells from the periphery need to cross the BBB. Additionally to enhanced endothelial permeability and BBB leakiness, inflammatory lesions are defined by astroglial activation as well as degradation and remodeling of the extracellular matrix [82].

Between the uncountable molecules of the ECM undergoing changes in neuroinflammation, one actor standing out may be the proteoglycan fibronectin (Fn), a multidomain glycoprotein binding to cell-surface-receptors, mostly integrins, and to the ECM. It appears in two forms: plasma Fn and intracellular Fn and is present in the matrices of most tissues [83]. Plasma Fn is produced by liver hepatocytes and released into the blood stream, where it plays an essential role for blood haemostasis. Cellular Fn (cFn) is released from migrating cells in diverse forms, generated by alternative splicing. cFn is secreted as a soluble covalent dimer and, in a complicated process in which the Fn molecule undergoes different conformational changes, is assembled into a stable matrix. This process of fibrillogenesis is not entirely identified, but it is most likely to function like a zipper, in which the Fn-molecules bind on specific domains, with some domains (the 70kDa) important for the initiation of the process and others (III1-2) for the stability of the binding [83].

In the context of perivascular inflammation in MS models, particularly Fn-integrin interactions seem to promote vascular remodeling during demyelinating disease [84]. Therefore, we investigated the relationship between viscoelastic changes of the brain and expression of Fn, as an indicator for remodeling of the NVU during lesion formation. Intriguingly, our data indicates that a reduction of brain viscoelasticity is associated with an overall increase of Fn expression in the brain tissue, which means higher levels of Fn were associated to a “softening” of the brain. Fn-fibrils within a matrix are under important tension, but when tension is removed, they relax to as little as one-quarter of their original length, for example, when one end of a fibril is released from is attachment site during tissue remodeling [85], a process common to EAE and MS. But although the Fn fibers are extremely elastic and might be expected to contribute to enhanced tissue elasticity, in this context their presence might reflect one aspect of a cascade of processes involved in disruption and reassembly of the neurovascular unit at lesion sites. Enhanced endothelial permeability, alteration of blood flow, enlargement of the perivascular spaces, inflammation, edema and astrocyte end feet detachment may ultimately lead to tissue softening. In our study, Fn gene expression also correlated

significantly with the amount of CD3e expression, supporting our hypothesis that fibril formation reflects ECM-remodeling processes linked to neuroinflammation. Importantly, we could reaffirm the correlation of Fn expression and reduced viscoelasticity in brain tissue from our previous study in SJL mice, in which MRE data was acquired in a coronal orientation [34]. Nonetheless, this correlation could not be extended to other ECM components, such as neurocan, brevican or glypican, which are known to be relevant for neuroinflammation, but presumably do not directly reflect processes of acute lesion formation [86, 87].

We found smaller amounts of Fn throughout the brain parenchyma, which suggests other sources of Fn than plasma-leakage. Indeed, our findings point towards a cellular origin of the deposits. Fn accumulations were associated to reactive astrocytes, which is in accordance with studies of other groups identifying astrocytes as major producers of the protein in demyelination [88]. However, further studies are required to determine the sources of Fn in neuroinflammatory models. Other cellular sources of the fibers are conceivable, and while we could reject T-cells as a Fn source (data not shown), we could not exclude other cells, such as brain endothelial cells, to be involved in the process.

BBB disruption involves multiple complex processes, that are not only limited to leakiness, i.e. endothelial permeability through TJ-degradation, but comprise further alterations of barrier-properties, such as breakdown of glia-limitans specific ECM through release of MMP-2 and MMP-9 [89], reduced astrocyte endfeet anchoring to the basement membrane as well as astrogliosis, facilitation of leukocyte migration [90] and ultimately formation of an astroglial scar. To further identify histopathological correlations of Fn accumulations, we performed immunofluorescence stainings of perivascular lesions in EAE mice. A combination of stainings for astrocytes, cell nuclei and Fn evidenced the degradation of the NVU with enhanced perivascular space and astrocyte endfoot detachment. Our stainings highlighted a complex disruption of the neurovascular junction, in which Fn deposits may only be one of many processes in a cascade of inflammation, barrier breakdown and reassembly, causing alterations of the brain mechanical properties, that we quantified in MRE measurements.

In chronically demyelinated MS lesions, Fn expression persists in aggregates, where it seems to be resistant to disassembly and contribute to remyelination failure. Conversely, remyelinated lesions of MS patients show no accumulations of Fn [52]. With the intention of gaining insight into Fn accumulations in later stages of EAE, we stained brain tissue of EAE mice at peak and remission phases of the disease. Fn accumulations were seen at both timepoints, but interestingly deposits at later stages were less confined to perivascular lesions and instead spread more diffusely into the surrounding parenchyma, and we hypothesize that a

clearance of Fn deposits from infiltrating immune and CNS resident cells causes this dispersion. Fn clearance is of central interest when thinking of ways to facilitate remyelination, and while latest research has shed light on some processes, a clear mechanism of Fn elimination has still to be depicted. Microglia and macrophages seem to be responsive to Fn aggregates in their phenotype, leaning towards a more pro-inflammatory instead of a remyelinating polarization when in contact to aggregated Fn [91]. At the same time, it has been shown that microglia- and macrophage-related MMP-7 cleaves Fn aggregates in a demyelination model and that reduced proMMP-levels contribute to their persistence in MS lesions [92]. Further research will be required to entirely understand the mechanisms in assembly and disassembly of Fn deposits and its importance in remyelination failure.

In summary, our work is part of a range of studies in animal models and MS patients elucidating the mechanisms around brain softening in neuroinflammatory diseases. In view of our data, we hypothesize that some of the alterations of brain mechanical properties we observed might be explained by remodeling processes around the BBB, such as enhancement of perivascular spaces and astrocyte endfoot detachment, debilitating connections between neuronal-vascular networks and leading to an overall loosening of brain tissue. This could also explain the comparably higher sensitivity of MRE to processes of acute neuroinflammation and lesion formation than GBCA-MRI. However, while we found intriguing changes of the ECM related to MRE alterations, further mechanisms related to barrier breakdown, especially in close up to the perivascular space, remain to be determined in future studies.

Conclusion

Altogether, the application of novel MRI techniques in mouse models of brain diseases is an emerging field, with potential of development. Nanoparticle-enhanced MRI and MRE are techniques that hold great promises and can complement conventional MRI. Nevertheless, due to the reduced size of a mouse brain – just about the size of a human thumb – improvements in spatial resolution and further technical developments that will allow faster acquisition with shorter scan times will be fundamental to gain further insight into the complex pathological mechanisms that neuroinflammation involves. Imaging of neuroinflammation is a wide field that has significantly shaped queries in MS research last years, and this study solely claims to gain insight into visualization of barrier-related aspects of neuroinflammation through the model of EAE. It is yet to find out how applicable the discussed methods are to the human brain, not least on account of the differences between a neuroinflammatory animal model and

the human MS condition. Eu-VSOP may be an excellent instrument to visualize pathophysiological processes around neuroinflammation and lesion formation, while their use in a clinical context is more unlikely for safety concerns. For MRE, a first step for the implementation as a diagnostic tool has been made, as use in human brain diseases has already taken place in several studies.

Until further research is done in humans, this work links in a multimodal investigation spatial and temporal changes of brain barriers to alterations of mechanical properties, vascular characteristics and molecular aspects of neuroinflammation. These insights lay a foundation to upcoming studies, in order to understand the pathophysiological processes taking place during neuroinflammation on one hand and on the other to eventually develop early diagnostic tools that allow sooner treatment, considerably improving life quality of affected persons.

REFERENCES

1. Reich, D.S., C.F. Lucchinetti, and P.A. Calabresi, *Multiple Sclerosis.* N Engl J Med, 2018. **378**(2): p. 169-180.
2. Vidal-Jordana, A. and X. Montalban, *Multiple Sclerosis: Epidemiologic, Clinical, and Therapeutic Aspects.* Neuroimaging Clin N Am, 2017. **27**(2): p. 195-204.
3. Baranzini, S.E. and J.R. Oksenberg, *The Genetics of Multiple Sclerosis: From 0 to 200 in 50 Years.* Trends Genet, 2017. **33**(12): p. 960-970.
4. Ascherio, A. and K.L. Munger, *Epidemiology of Multiple Sclerosis: From Risk Factors to Prevention-An Update.* Semin Neurol, 2016. **36**(2): p. 103-14.
5. Brownlee, W.J., T.A. Hardy, F. Fazekas, and D.H. Miller, *Diagnosis of multiple sclerosis: progress and challenges.* Lancet, 2017. **389**(10076): p. 1336-1346.
6. Buzzard, K., W.H. Chan, T. Kilpatrick, and S. Murray, *Multiple Sclerosis: Basic and Clinical.* Adv Neurobiol, 2017. **15**: p. 211-252.
7. Stadelmann, C., C. Wegner, and W. Bruck, *Inflammation, demyelination, and degeneration - recent insights from MS pathology.* Biochim Biophys Acta, 2011. **1812**(2): p. 275-82.
8. Stys, P.K., G.W. Zamponi, J. van Minnen, and J.J. Geurts, *Will the real multiple sclerosis please stand up?* Nat Rev Neurosci, 2012. **13**(7): p. 507-14.
9. Sawcer, S., G. Hellenthal, M. Pirinen, C.C. Spencer, N.A. Patsopoulos, L. Moutsianas, A. Dilthey, Z. Su, C. Freeman, S.E. Hunt, S. Edkins, E. Gray, D.R. Booth, S.C. Potter, A. Goris, G. Band, A.B. Oturai, A. Strange, J. Saarela, C. Bellenguez, B. Fontaine, M. Gillman, B. Hemmer, R. Gwilliam, F. Zipp, A. Jayakumar, R. Martin, S. Leslie, S. Hawkins, E. Giannoulatou, S. D'Alfonso, H. Blackburn, F. Martinelli Boneschi, J. Liddle, H.F. Harbo, M.L. Perez, A. Spurkland, M.J. Waller, M.P. Mycko, M. Ricketts, M. Comabella, N. Hammond, I. Kockum, O.T. McCann, M. Ban, P. Whittaker, A. Kemppinen, P. Weston, C. Hawkins, S. Widaa, J. Zajicek, S. Dronov, N. Robertson, S.J. Bumpstead, L.F. Barcellos, R. Ravindrarajah, R. Abraham, L. Alfredsson, K. Ardlie, C. Aubin, A. Baker, K. Baker, S.E. Baranzini, L. Bergamaschi, R. Bergamaschi, A. Bernstein, A. Berthele, M. Boggild, J.P. Bradfield, D. Brassat, S.A. Broadley, D. Buck, H. Butzkueven, R. Capra, W.M. Carroll, P. Cavalla, E.G. Celius, S. Cepok, R. Chiavacci, F. Clerget-Darpoux, K. Clysters, G. Comi, M. Cossburn, I. Cournu-Rebeix, M.B. Cox, W. Cozen, B.A. Cree, A.H. Cross, D. Cusi, M.J. Daly, E. Davis, P.I. de

Bakker, M. Debouverie, B. D'Hooghe M, K. Dixon, R. Dobosi, B. Dubois, D. Ellinghaus, I. Elovaara, F. Esposito, C. Fontenille, S. Foote, A. Franke, D. Galimberti, A. Ghezzi, J. Glessner, R. Gomez, O. Gout, C. Graham, S.F. Grant, F.R. Guerini, H. Hakonarson, P. Hall, A. Hamsten, H.P. Hartung, R.N. Heard, S. Heath, J. Hobart, M. Hoshi, C. Infante-Duarte, G. Ingram, W. Ingram, T. Islam, M. Jagodic, M. Kabesch, A.G. Kermode, T.J. Kilpatrick, C. Kim, N. Klopp, K. Koivisto, M. Larsson, M. Lathrop, J.S. Lechner-Scott, M.A. Leone, V. Leppa, U. Liljedahl, I.L. Bomfim, R.R. Lincoln, J. Link, J. Liu, A.R. Lorentzen, S. Lupoli, F. Macciardi, T. Mack, M. Marriott, V. Martinelli, D. Mason, J.L. McCauley, F. Mentch, I.L. Mero, T. Mihalova, X. Montalban, J. Mottershead, K.M. Myhr, P. Naldi, W. Ollier, A. Page, A. Palotie, J. Pelletier, L. Piccio, T. Pickersgill, F. Piehl, S. Pobywajlo, H.L. Quach, P.P. Ramsay, M. Reunanen, R. Reynolds, J.D. Rioux, M. Rodegher, S. Roesner, J.P. Rubio, I.M. Ruckert, M. Salvetti, E. Salvi, A. Santaniello, C.A. Schaefer, S. Schreiber, C. Schulze, R.J. Scott, F. Sellebjerg, K.W. Selmaj, D. Sexton, L. Shen, B. Simms-Acuna, S. Skidmore, P.M. Sleiman, C. Smestad, P.S. Sorensen, H.B. Sondergaard, J. Stankovich, R.C. Strange, A.M. Sulonen, E. Sundqvist, A.C. Syvanen, F. Taddeo, B. Taylor, J.M. Blackwell, P. Tienari, E. Bramon, A. Tourbah, M.A. Brown, E. Tronczynska, J.P. Casas, N. Tubridy, A. Corvin, J. Vickery, J. Jankowski, P. Villoslada, H.S. Markus, K. Wang, C.G. Mathew, J. Wason, C.N. Palmer, H.E. Wichmann, R. Plomin, E. Willoughby, A. Rautanen, J. Winkelmann, M. Wittig, R.C. Trembath, J. Yaouanq, A.C. Viswanathan, H. Zhang, N.W. Wood, R. Zuvich, P. Deloukas, C. Langford, A. Duncanson, J.R. Oksenberg, M.A. Pericak-Vance, J.L. Haines, T. Olsson, J. Hillert, A.J. Ivinson, P.L. De Jager, L. Peltonen, G.J. Stewart, D.A. Hafler, S.L. Hauser, G. McVean, P. Donnelly and A. Compston, *Genetic risk and a primary role for cell-mediated immune mechanisms in multiple sclerosis.* Nature, 2011. **476**(7359): p. 214-9.

10. Heneka, M.T., M.P. Kummer, and E. Latz, *Innate immune activation in neurodegenerative disease.* Nat Rev Immunol, 2014. **14**(7): p. 463-77.
11. Moll, N.M., A.M. Rietsch, S. Thomas, A.J. Ransohoff, J.C. Lee, R. Fox, A. Chang, R.M. Ransohoff, and E. Fisher, *Multiple sclerosis normal-appearing white matter: pathology-imaging correlations.* Ann Neurol, 2011. **70**(5): p. 764-73.
12. Dendrou, C.A., L. Fugger, and M.A. Friese, *Immunopathology of multiple sclerosis.* Nat Rev Immunol, 2015. **15**(9): p. 545-58.
13. Scheikl, T., B. Pignolet, L.T. Mars, and R.S. Liblau, *Transgenic mouse models of multiple sclerosis.* Cell Mol Life Sci, 2010. **67**(23): p. 4011-34.

14. Robinson, A.P., C.T. Harp, A. Noronha, and S.D. Miller, *The experimental autoimmune encephalomyelitis (EAE) model of MS: utility for understanding disease pathophysiology and treatment.* Handb Clin Neurol, 2014. **122**: p. 173-89.
15. Spencer, J.I., J.S. Bell, and G.C. DeLuca, *Vascular pathology in multiple sclerosis: reframing pathogenesis around the blood-brain barrier.* J Neurol Neurosurg Psychiatry, 2018. **89**(1): p. 42-52.
16. Yadav, S.K., J.E. Mindur, K. Ito, and S. Dhib-Jalbut, *Advances in the immunopathogenesis of multiple sclerosis.* Curr Opin Neurol, 2015. **28**(3): p. 206-19.
17. Reboldi, A., C. Coisne, D. Baumjohann, F. Benvenuto, D. Bottinelli, S. Lira, A. Uccelli, A. Lanzavecchia, B. Engelhardt, and F. Sallusto, *C-C chemokine receptor 6-regulated entry of TH-17 cells into the CNS through the choroid plexus is required for the initiation of EAE.* Nat Immunol, 2009. **10**(5): p. 514-23.
18. Engelhardt, B., K. Wolburg-Buchholz, and H. Wolburg, *Involvement of the choroid plexus in central nervous system inflammation.* Microsc Res Tech, 2001. **52**(1): p. 112-29.
19. Ubogu, E.E., M.B. Cossoy, and R.M. Ransohoff, *The expression and function of chemokines involved in CNS inflammation.* Trends Pharmacol Sci, 2006. **27**(1): p. 48-55.
20. Chard, D. and S.A. Trip, *Resolving the clinico-radiological paradox in multiple sclerosis.* F1000Res, 2017. **6**: p. 1828.
21. Przybek, J., I. Gniatkowska, D. Mirowska-Guzel, and A. Czlonkowska, *Evolution of diagnostic criteria for multiple sclerosis.* Neurol Neurochir Pol, 2015. **49**(5): p. 313-21.
22. Davis, F.A., *The clinico-radiological paradox in multiple sclerosis: novel implications of lesion size.* Multiple Sclerosis Journal, 2013. **20**(4): p. 515-516.
23. Wuerfel, J., E. Tysiak, T. Prozorovski, M. Smyth, S. Mueller, J. Schnorr, M. Taupitz, and F. Zipp, *Mouse model mimics multiple sclerosis in the clinico-radiological paradox.* Eur J Neurosci, 2007. **26**(1): p. 190-8.
24. Vellinga, M.M., R.D. Oude Engberink, A. Seewann, P.J. Pouwels, M.P. Wattjes, S.M. van der Pol, C. Pering, C.H. Polman, H.E. de Vries, J.J. Geurts, and F. Barkhof, *Pluriformity of inflammation in multiple sclerosis shown by ultra-small iron oxide particle enhancement.* Brain, 2008. **131**(Pt 3): p. 800-7.
25. Wagner, S., J. Schnorr, H. Pilgrimm, B. Hamm, and M. Taupitz, *Monomer-coated very small superparamagnetic iron oxide particles as contrast medium for magnetic resonance imaging: preclinical in vivo characterization.* Invest Radiol, 2002. **37**(4): p. 167-77.

26. Lunov, O., T. Syrovets, C. Rocker, K. Tron, G.U. Nienhaus, V. Rasche, V. Mailander, K. Landfester, and T. Simmet, *Lysosomal degradation of the carboxydextran shell of coated superparamagnetic iron oxide nanoparticles and the fate of professional phagocytes.* Biomaterials, 2010. **31**(34): p. 9015-22.
27. Tysiak, E., P. Asbach, O. Aktas, H. Waiczies, M. Smyth, J. Schnorr, M. Taupitz, and J. Wuerfel, *Beyond blood brain barrier breakdown - in vivo detection of occult neuroinflammatory foci by magnetic nanoparticles in high field MRI.* J Neuroinflammation, 2009. **6**: p. 20.
28. Millward, J.M., J. Schnorr, M. Taupitz, S. Wagner, J.T. Wuerfel, and C. Infante-Duarte, *Iron oxide magnetic nanoparticles highlight early involvement of the choroid plexus in central nervous system inflammation.* ASN Neuro, 2013. **5**(1): p. e00110.
29. Berndt, D., J.M. Millward, J. Schnorr, M. Taupitz, V. Stangl, F. Paul, S. Wagner, J.T. Wuerfel, I. Sack, A. Ludwig, and C. Infante-Duarte, *Inflammation-induced brain endothelial activation leads to uptake of electrostatically stabilized iron oxide nanoparticles via sulfated glycosaminoglycans.* Nanomedicine, 2017. **13**(4): p. 1411-1421.
30. Gulani, V., F. Calamante, F.G. Shellock, E. Kanal, and S.B. Reeder, *Gadolinium deposition in the brain: summary of evidence and recommendations.* Lancet Neurol, 2017. **16**(7): p. 564-570.
31. Wang, S., B. Hesse, M. Roman, D. Stier, H. Castillo-Michel, M. Cotte, J.P. Suuronen, A. Lagrange, H. Radbruch, F. Paul, M. Taupitz, E. Schellenberger, I. Sack, and C. Infante-Duarte, *Increased Retention of Gadolinium in the Inflamed Brain After Repeated Administration of Gadopentetate Dimeglumine: A Proof-of-Concept Study in Mice Combining ICP-MS and Micro- and Nano-SR-XRF.* Invest Radiol, 2019.
32. Mariappan, Y.K., K.J. Glaser, and R.L. Ehman, *Magnetic resonance elastography: a review.* Clin Anat, 2010. **23**(5): p. 497-511.
33. Asbach, P., D. Klatt, B. Schlosser, M. Biermer, M. Muche, A. Rieger, C. Loddenkemper, R. Somasundaram, T. Berg, B. Hamm, J. Braun, and I. Sack, *Viscoelasticity-based staging of hepatic fibrosis with multifrequency MR elastography.* Radiology, 2010. **257**(1): p. 80-6.
34. Riek, K., J.M. Millward, I. Hamann, S. Mueller, C.F. Pfueller, F. Paul, J. Braun, C. Infante-Duarte, and I. Sack, *Magnetic resonance elastography reveals altered brain viscoelasticity in experimental autoimmune encephalomyelitis.* Neuroimage Clin, 2012. **1**(1): p. 81-90.

35. Sack, I., K.J. Streitberger, D. Krefting, F. Paul, and J. Braun, *The influence of physiological aging and atrophy on brain viscoelastic properties in humans.* PLoS One, 2011. **6**(9): p. e23451.
36. Murphy, M.C., J. Huston, 3rd, C.R. Jack, Jr., K.J. Glaser, A. Manduca, J.P. Felmlee, and R.L. Ehman, *Decreased brain stiffness in Alzheimer's disease determined by magnetic resonance elastography.* J Magn Reson Imaging, 2011. **34**(3): p. 494-8.
37. Lipp, A., R. Trbojevic, F. Paul, A. Fehlner, S. Hirsch, M. Scheel, C. Noack, J. Braun, and I. Sack, *Cerebral magnetic resonance elastography in supranuclear palsy and idiopathic Parkinson's disease.* Neuroimage Clin, 2013. **3**: p. 381-7.
38. Streitberger, K.J., E. Wiener, J. Hoffmann, F.B. Freimann, D. Klatt, J. Braun, K. Lin, J. McLaughlin, C. Sprung, R. Klingebiel, and I. Sack, *In vivo viscoelastic properties of the brain in normal pressure hydrocephalus.* NMR Biomed, 2011. **24**(4): p. 385-92.
39. Fehlner, A., J.R. Behrens, K.J. Streitberger, S. Papazoglou, J. Braun, J. Bellmann-Strobl, K. Ruprecht, F. Paul, J. Wurfel, and I. Sack, *Higher-resolution MR elastography reveals early mechanical signatures of neuroinflammation in patients with clinically isolated syndrome.* J Magn Reson Imaging, 2016. **44**(1): p. 51-8.
40. Streitberger, K.J., I. Sack, D. Krefting, C. Pfuller, J. Braun, F. Paul, and J. Wuerfel, *Brain viscoelasticity alteration in chronic-progressive multiple sclerosis.* PLoS One, 2012. **7**(1): p. e29888.
41. Wuerfel, J., F. Paul, B. Beierbach, U. Hamhaber, D. Klatt, S. Papazoglou, F. Zipp, P. Martus, J. Braun, and I. Sack, *MR-elastography reveals degradation of tissue integrity in multiple sclerosis.* Neuroimage, 2010. **49**(3): p. 2520-5.
42. Streitberger, K.J., A. Fehlner, F. Pache, A. Lacheta, S. Papazoglou, J. Bellmann-Strobl, K. Ruprecht, A. Brandt, J. Braun, I. Sack, F. Paul, and J. Wuerfel, *Multifrequency magnetic resonance elastography of the brain reveals tissue degeneration in neuromyelitis optica spectrum disorder.* Eur Radiol, 2017. **27**(5): p. 2206-2215.
43. Schregel, K., E. Wuerfel, P. Garteiser, I. Gemeinhardt, T. Prozorovski, O. Aktas, H. Merz, D. Petersen, J. Wuerfel, and R. Sinkus, *Demyelination reduces brain parenchymal stiffness quantified in vivo by magnetic resonance elastography.* Proc Natl Acad Sci U S A, 2012. **109**(17): p. 6650-5.
44. Millward, J.M., J. Guo, D. Berndt, J. Braun, I. Sack, and C. Infante-Duarte, *Tissue structure and inflammatory processes shape viscoelastic properties of the mouse brain.* NMR Biomed, 2015. **28**(7): p. 831-9.

45. Bandtlow, C.E. and D.R. Zimmermann, *Proteoglycans in the Developing Brain: New Conceptual Insights for Old Proteins.* 2000.
46. Szuchet, S., K. Watanabe, and Y. Yamaguchi, *Differentiation/regeneration of oligodendrocytes entails the assembly of a cell-associated matrix.* Int J Dev Neurosci, 2000. **18**(7): p. 705-20.
47. Pires Neto, M.A., S. Braga-de-Souza, and R. Lent, *Extracellular matrix molecules play diverse roles in the growth and guidance of central nervous system axons.* Braz J Med Biol Res, 1999. **32**(5): p. 633-8.
48. Colognato, H., S. Ramachandrappa, I.M. Olsen, and C. ffrench-Constant, *Integrins direct Src family kinases to regulate distinct phases of oligodendrocyte development*, in *J Cell Biol*. 2004. p. 365-75.
49. Sobel, R.A. and A.S. Ahmed, *White matter extracellular matrix chondroitin sulfate/dermatan sulfate proteoglycans in multiple sclerosis.* J Neuropathol Exp Neurol, 2001. **60**(12): p. 1198-207.
50. Back, S.A., T.M. Tuohy, H. Chen, N. Wallingford, A. Craig, J. Struve, N.L. Luo, F. Banine, Y. Liu, A. Chang, B.D. Trapp, B.F. Bebo, Jr., M.S. Rao, and L.S. Sherman, *Hyaluronan accumulates in demyelinated lesions and inhibits oligodendrocyte progenitor maturation.* Nat Med, 2005. **11**(9): p. 966-72.
51. van Horssen, J., L. Bo, C.D. Dijkstra, and H.E. de Vries, *Extensive extracellular matrix depositions in active multiple sclerosis lesions.* Neurobiol Dis, 2006. **24**(3): p. 484-91.
52. Stoffels, J.M., J.C. de Jonge, M. Stancic, A. Nomden, M.E. van Strien, D. Ma, Z. Siskova, O. Maier, C. Ffrench-Constant, R.J. Franklin, D. Hoekstra, C. Zhao, and W. Baron, *Fibronectin aggregation in multiple sclerosis lesions impairs remyelination.* Brain, 2013. **136**(Pt 1): p. 116-31.
53. Mohan, H., M. Krumbholz, R. Sharma, S. Eisele, A. Junker, M. Sixt, J. Newcombe, H. Wekerle, R. Hohlfeld, H. Lassmann, and E. Meinl, *Extracellular matrix in multiple sclerosis lesions: Fibrillar collagens, biglycan and decorin are upregulated and associated with infiltrating immune cells.* Brain Pathol, 2010. **20**(5): p. 966-75.
54. Galtrey, C.M. and J.W. Fawcett, *The role of chondroitin sulfate proteoglycans in regeneration and plasticity in the central nervous system.* Brain Res Rev, 2007. **54**(1): p. 1-18.
55. Chun, S.J., M.N. Rasband, R.L. Sidman, A.A. Habib, and T. Vartanian, *Integrin-linked kinase is required for laminin-2-induced oligodendrocyte cell spreading and CNS myelination.* J Cell Biol, 2003. **163**(2): p. 397-408.

56. Colognato, H., C. ffrench-Constant, and M.L. Feltri, *Human diseases reveal novel roles for neural laminins.* Trends Neurosci, 2005. **28**(9): p. 480-6.
57. Sobel, R.A. and M.E. Mitchell, *Fibronectin in multiple sclerosis lesions.* Am J Pathol, 1989. **135**(1): p. 161-8.
58. Millward, J.M., A. Ariza de Schellenberger, D. Berndt, L. Hanke-Vela, E. Schellenberger, S. Waiczies, M. Taupitz, Y. Kobayashi, S. Wagner, and C. Infante-Duarte, *Application of Europium-Doped Very Small Iron Oxide Nanoparticles to Visualize Neuroinflammation with MRI and Fluorescence Microscopy.* Neuroscience, 2017.
59. Kobayashi, Y., R. Hauptmann, H. Kratz, M. Ebert, S. Wagner, and M. Taupitz, *Europium doping of superparamagnetic iron oxide nanoparticles enables their detection by fluorescence microscopy and for quantitative analytics.* Technol Health Care, 2016.
60. Scharlach, C., L. Müller, S. Wagner, Y. Kobayashi, H. Kratz, M. Ebert, N. Jakubowski, and E. Schellenberger, *LA-ICP-MS Allows Quantitative Microscopy of Europium-Doped Iron Oxide Nanoparticles and is a Possible Alternative to Ambiguous Prussian Blue Iron Staining.* J Biomed Nanotechnol, 2016. **12**(5): p. 1001-10.
61. de Schellenberger, A.A., R. Hauptmann, J.M. Millward, E. Schellenberger, Y. Kobayashi, M. Taupitz, C. Infante-Duarte, J. Schnorr, and S. Wagner, *Synthesis of europium-doped VSOP, customized enhancer solution and improved microscopy fluorescence methodology for unambiguous histological detection.* J Nanobiotechnology, 2017. **15**(1): p. 71.
62. Sack, I., K. Jöhrens, J. Wuerfel, and J. Braun, *Structure-sensitive elastography: on the viscoelastic powerlaw behavior of in vivo human tissue in health and disease.* Soft Matter 2013. **9**: p. 5672-5680.
63. Hibbits, N., J. Yoshino, T.Q. Le, and R.C. Armstrong, *Astrogliosis during acute and chronic cuprizone demyelination and implications for remyelination.* ASN Neuro, 2012. **4**(6): p. 393-408.
64. Han, G., Y. Deng, J. Sun, J. Ling, and Z. Shen, *Research into europium complexes as magnetic resonance imaging contrast agents (Review).* Exp Ther Med, 2015. **9**(5): p. 1561-1566.
65. Carron, S., M. Bloemen, L. Vander Elst, S. Laurent, T. Verbiest, and T.N. Parac-Vogt, *Ultrasmall Superparamagnetic Iron Oxide Nanoparticles with Europium(III) DO3A as a Bimodal Imaging Probe.* Chemistry, 2016. **22**(13): p. 4521-7.
66. Kobayashi, Y., R. Hauptmann, H. Kratz, M. Ebert, S. Wagner, and M. Taupitz, *Europium doping of superparamagnetic iron oxide nanoparticles enables their detection by*

fluorescence microscopy and for quantitative analytics. Technol Health Care, 2017. **25**(3): p. 457-470.

67. Rausch, M., P. Hiestand, D. Baumann, C. Cannet, and M. Rudin, *MRI-based monitoring of inflammation and tissue damage in acute and chronic relapsing EAE.* Magn Reson Med, 2003. **50**(2): p. 309-14.
68. Berger, C., P. Hiestand, D. Kindler-Baumann, M. Rudin, and M. Rausch, *Analysis of lesion development during acute inflammation and remission in a rat model of experimental autoimmune encephalomyelitis by visualization of macrophage infiltration, demyelination and blood-brain barrier damage.* NMR Biomed, 2006. **19**(1): p. 101-7.
69. Brochet, B., M.S. Deloire, T. Touil, O. Anne, J.M. Caille, V. Dousset, and K.G. Petry, *Early macrophage MRI of inflammatory lesions predicts lesion severity and disease development in relapsing EAE.* Neuroimage, 2006. **32**(1): p. 266-74.
70. Zhang, Y., J. Wells, R. Buist, J. Peeling, V.W. Yong, and J.R. Mitchell, *Active inflammation increases the heterogeneity of MRI texture in mice with relapsing experimental allergic encephalomyelitis.* Magn Reson Imaging, 2014. **32**(2): p. 168-74.
71. Lopes Pinheiro, M.A., G. Kooij, M.R. Mizee, A. Kamermans, G. Enzmann, R. Lyck, M. Schwaninger, B. Engelhardt, and H.E. de Vries, *Immune cell trafficking across the barriers of the central nervous system in multiple sclerosis and stroke.* Biochim Biophys Acta, 2016. **1862**(3): p. 461-71.
72. Cepok, S., M. Jacobsen, S. Schock, B. Omer, S. Jaekel, I. Boddeker, W.H. Oertel, N. Sommer, and B. Hemmer, *Patterns of cerebrospinal fluid pathology correlate with disease progression in multiple sclerosis.* Brain, 2001. **124**(Pt 11): p. 2169-76.
73. Kunis, G., K. Baruch, N. Rosenzweig, A. Kertser, O. Miller, T. Berkutzki, and M. Schwartz, *IFN-gamma-dependent activation of the brain's choroid plexus for CNS immune surveillance and repair.* Brain, 2013. **136**(Pt 11): p. 3427-40.
74. Steffen, B.J., G. Breier, E.C. Butcher, M. Schulz, and B. Engelhardt, *ICAM-1, VCAM-1, and MAdCAM-1 are expressed on choroid plexus epithelium but not endothelium and mediate binding of lymphocytes in vitro.* Am J Pathol, 1996. **148**(6): p. 1819-38.
75. Zhang, X., C. Wu, J. Song, M. Gotte, and L. Sorokin, *Syndecan-1, a cell surface proteoglycan, negatively regulates initial leukocyte recruitment to the brain across the choroid plexus in murine experimental autoimmune encephalomyelitis.* J Immunol, 2013. **191**(9): p. 4551-61.

76. Shrestha, B., D. Paul, and J.S. Pachter, *Alterations in tight junction protein and IgG permeability accompany leukocyte extravasation across the choroid plexus during neuroinflammation.* J Neuropathol Exp Neurol, 2014. **73**(11): p. 1047-61.
77. Kooij, G., K. Kopplin, R. Blasig, M. Stuiver, N. Koning, G. Goverse, S.M. van der Pol, B. van Het Hof, M. Gollasch, J.A. Drexhage, A. Reijerkerk, I.C. Meij, R. Mebius, T.E. Willnow, D. Muller, I.E. Blasig, and H.E. de Vries, *Disturbed function of the blood-cerebrospinal fluid barrier aggravates neuro-inflammation.* Acta Neuropathol, 2014. **128**(2): p. 267-77.
78. Strazielle, N. and J.F. Ghersi-Egea, *Potential Pathways for CNS Drug Delivery Across the Blood-Cerebrospinal Fluid Barrier.* Curr Pharm Des, 2016. **22**(35): p. 5463-5476.
79. Zhang, J., M.A. Green, R. Sinkus, and L.E. Bilston, *Viscoelastic properties of human cerebellum using magnetic resonance elastography.* J Biomech, 2011. **44**(10): p. 1909-13.
80. Tonra, J.R., *Cerebellar susceptibility to experimental autoimmune encephalomyelitis in SJL/J mice: potential interaction of immunology with vascular anatomy.* Cerebellum, 2002. **1**(1): p. 57-68.
81. Herrmann, K., B.O. Erokwu, M.L. Johansen, J.P. Basilion, V. Gulani, M.A. Griswold, C.A. Flask, and S.M. Brady-Kalnay, *Dynamic Quantitative T1 Mapping in Orthotopic Brain Tumor Xenografts.* Transl Oncol, 2016. **9**(2): p. 147-154.
82. Voskuhl, R.R., R.S. Peterson, B. Song, Y. Ao, L.B. Morales, S. Tiwari-Woodruff, and M.V. Sofroniew, *Reactive astrocytes form scar-like perivascular barriers to leukocytes during adaptive immune inflammation of the CNS.* J Neurosci, 2009. **29**(37): p. 11511-22.
83. Schwarzbauer, J.E. and D.W. DeSimone, *Fibronectins, their fibrillogenesis, and in vivo functions.* Cold Spring Harb Perspect Biol, 2011. **3**(7).
84. Boroujerdi, A., J.V. Welser-Alves, and R. Milner, *Extensive vascular remodeling in the spinal cord of pre-symptomatic experimental autoimmune encephalomyelitis mice; increased vessel expression of fibronectin and the alpha5beta1 integrin.* Exp Neurol, 2013. **250**: p. 43-51.
85. Ohashi, T., D.P. Kiehart, and H.P. Erickson, *Dynamics and elasticity of the fibronectin matrix in living cell culture visualized by fibronectin-green fluorescent protein.* Proc Natl Acad Sci U S A, 1999. **96**(5): p. 2153-8.

86. Haylock-Jacobs, S., M.B. Keough, L. Lau, and V.W. Yong, *Chondroitin sulphate proteoglycans: extracellular matrix proteins that regulate immunity of the central nervous system.* Autoimmun Rev, 2011. **10**(12): p. 766-72.
87. Lorentzen, A.R., E. Melum, E. Ellinghaus, C. Smestad, I.L. Mero, J.H. Aarseth, K.M. Myhr, E.G. Celius, B.A. Lie, T.H. Karlsen, A. Franke, and H.F. Harbo, *Association to the Glypican-5 gene in multiple sclerosis.* J Neuroimmunol, 2010. **226**(1-2): p. 194-7.
88. Stoffels, J.M., D. Hoekstra, R.J. Franklin, W. Baron, and C. Zhao, *The EIIIA domain from astrocyte-derived fibronectin mediates proliferation of oligodendrocyte progenitor cells following CNS demyelination.* Glia, 2015. **63**(2): p. 242-56.
89. Song, J., C. Wu, E. Korpos, X. Zhang, S.M. Agrawal, Y. Wang, C. Faber, M. Schafers, H. Korner, G. Opdenakker, R. Hallmann, and L. Sorokin, *Focal MMP-2 and MMP-9 activity at the blood-brain barrier promotes chemokine-induced leukocyte migration.* Cell Rep, 2015. **10**(7): p. 1040-54.
90. Gimenez, M.A., J.E. Sim, and J.H. Russell, *TNFR1-dependent VCAM-1 expression by astrocytes exposes the CNS to destructive inflammation.* J Neuroimmunol, 2004. **151**(1-2): p. 116-25.
91. Sikkema, A.H., J.M.J. Stoffels, P. Wang, F.J. Basedow, R. Bulsink, J.J. Bajramovic, and W. Baron, *Fibronectin aggregates promote features of a classically and alternatively activated phenotype in macrophages.* J Neuroinflammation, 2018. **15**(1): p. 218.
92. Wang, P., R.P. Gorter, J.C. de Jonge, M. Nazmuddin, C. Zhao, S. Amor, D. Hoekstra, and W. Baron, *MMP7 cleaves remyelination-impairing fibronectin aggregates and its expression is reduced in chronic multiple sclerosis lesions.* Glia, 2018. **66**(8): p. 1625-1643.

AFFIDAVIT / EIDESSTATTLICHE VERSICHERUNG

„Ich, Laura Hanke Vela, versichere an Eides statt durch meine eigenhändige Unterschrift, dass ich die vorgelegte Dissertation mit dem Thema: „Novel MR Tools Highlight Brain Barrier Alterations in a Mouse Model of Multiple Sclerosis“ selbstständig und ohne nicht offengelegte Hilfe Dritter verfasst und keine anderen als die angegebenen Quellen und Hilfsmittel genutzt habe.

Alle Stellen, die wörtlich oder dem Sinne nach auf Publikationen oder Vorträgen anderer AutorInnen beruhen, sind als solche in korrekter Zitierung kenntlich gemacht. Die Abschnitte zu Methodik (insbesondere praktische Arbeiten, Laborbestimmungen, statistische Aufarbeitung) und Resultaten (insbesondere Abbildungen, Grafiken und Tabellen) werden von mir verantwortet.

Meine Anteile an etwaigen Publikationen zu dieser Dissertation entsprechen denen, die in der untenstehenden gemeinsamen Erklärung mit der Betreuerin, angegeben sind. Für sämtliche im Rahmen der Dissertation entstandenen Publikationen wurden die Richtlinien des ICMJE (International Committee of Medical Journal Editors; www.icmje.og) zur Autorenschaft eingehalten. Ich erkläre ferner, dass mir die Satzung der Charité – Universitätsmedizin Berlin zur Sicherung Guter Wissenschaftlicher Praxis bekannt ist und ich mich zur Einhaltung dieser Satzung verpflichte.

Die Bedeutung dieser eidesstattlichen Versicherung und die strafrechtlichen Folgen einer unwahren eidesstattlichen Versicherung (§§156, 161 des Strafgesetzbuches) sind mir bekannt und bewusst.“

Berlin, den 25.06.2019

Unterschrift

CONTRIBUTION ON PUBLICATIONS / ANTEILSERKLÄRUNG AN ERFOLGTEN PUBLIKATIONEN

Laura Hanke Vela hatte folgenden Anteil an den folgenden Publikationen:

Publikation 1:

Application of Europium-Doped Very Small Iron Oxide Nanoparticles to Visualize Neuroinflammation with MRI and Fluorescence Microscopy. Millward, J.M., A. Ariza de Schellenberger, D. Berndt, L. Hanke-Vela, E. Schellenberger, S. Waiczies, M. Taupitz, Y. Kobayashi, S. Wagner, and C. Infante-Duarte, *Neuroscience,* 2017.

Beitrag im Einzelnen:

Experimenteller Teil:

- In vivo: Monitoring von EAE Mäusen, Assistenz bei i.v. Prozeduren und MR-Messungen
- In vitro: Assistenz und Pflege der Zellkulturen
- Präparation und histologische Aufarbeitung der Mäusehirne in Zusammenarbeit mit J.M. Millward
- Anfertigung von Übersichtsfärbungen und Einschätzung von Regions of Interest
- Anfertigung und Analyse von Immunfluoreszenzfärbungen

_____

Unterschrift, Datum und Stempel der betreuenden Hochschullehrerin

_____

Unterschrift der Doktorandin

CURRICULUM VITAE

Mein Lebenslauf wird aus datenschutzrechtlichen Gründen in der elektronischen Version meiner Arbeit nicht veröffentlicht.

LIST OF PUBLICATIONS

Application of Europium-Doped Very Small Iron Oxide Nanoparticles to Visualize Neuroinflammation with MRI and Fluorescence Microscopy. Millward, J.M., A. Ariza de Schellenberger, D. Berndt, L. Hanke-Vela, E. Schellenberger, S. Waiczies, M. Taupitz, Y. Kobayashi, S. Wagner, and C. Infante-Duarte, *Neuroscience,* 2017.

ACKNOWLEDGEMENTS

I would like to express my great appreciation to my supervisor PD Dr. Carmen Infante-Duarte, who has led me through the planning and development of this project with valuable and constructive suggestions. Her willingness to spend her time so generously, sharing her immense knowledge and the love to her work has been encouraging during this whole project. I would also like to express my gratitude to Dr. Jason Millward, who introduced me into the experimental work, inciting my interest in the matter by long chats and evenings at the microscope. His enthusiasm for scientific research has been a great motivation. My grateful thanks are extended to Natascha Asselborn, whose experience in the laboratory was very much appreciated, and to Shuangqing Wang and the rest of the Infante-Duarte group, whom I have had the pleasure to work with during this project. I would like to thank my parents and brother for the support and patience provided during the last years in my work and life in general and my friends for supporting me spiritually, especially Victoria Stampfer for her creative assistance with the illustrations in this report.